

**MoVO-based catalysts for the oxidation of ethane to ethylene and acetic acid. Influence of niobium and/or palladium on physicochemical and catalytic properties.**

Martial Roussel<sup>1</sup>, Michel Bouchard<sup>1</sup>, Khalid Karim<sup>2</sup>, Saleh Al-Sayari<sup>2</sup>,  
Elisabeth Bordes-Richard<sup>1\*</sup>

<sup>1</sup>: *Unité de Catalyse et de Chimie du Solide, UMR CNRS 8181, USTL-ENSCL-ECL, Cité Scientifique, 59655 Villeneuve d'Ascq Cedex, France*

<sup>2</sup>: *SABIC R&T, P.O. Box 42503, Riyadh, Saudi Arabia*

\* Corresponding author:      Tel: +33 (0)3 20 43 45 26

Fax: +33 (0)3 20 43 65 61

Mail: [Elisabeth.Bordes@univ-lille1.fr](mailto:Elisabeth.Bordes@univ-lille1.fr)

## ABSTRACT

The influence of niobium and/or palladium in  $\text{MoV}_{0.4}\text{O}_x$  on both solid state chemistry and catalytic properties in the oxidation of ethane to acetic acid and ethylene is examined. Catalysts without molybdenum ( $\text{VNb}_{0.31}\text{Pd}_{3e-4}\text{O}_x$ ) are also studied for comparison. The structural properties of the precursors and of the catalysts obtained by calcination of precursors at 350 and 400°C are studied by X-ray diffraction, and by laser Raman and X-ray photoelectron spectroscopies. These properties depend on the presence or absence of niobium, and to a lesser extent, of palladium. Nb-free precursors and catalysts are heterogeneous mixtures of crystalline oxides, among which hexagonal and orthorhombic  $\text{MoO}_3$ . The presence of Pd favors the instability of both precursors and catalysts. The catalysts are poorly active (conversion < 4%), but they are mainly selective to acetic acid ( $S_{\text{AA max}} = 61\text{-}73$  mol%) and to  $\text{CO}_x$  ( $S_{\text{COx max}} = 30\text{-}72$  mol%). The Nb-containing precursors without or with Pd are more stable, and the catalysts are made up of nanocrystalline particles of V,Nb-doped  $\text{Mo}_5\text{O}_{14}$  and of  $\text{V}_x\text{Mo}_{1-x}\text{O}_{3-x/2}$ . They are active (conversion < 15%) and very selective to ethylene and acetic acid ( $S_{\text{tot}} = 90\text{-}96$  mol%). The surface being enriched with vanadium in most cases, the discussion deals with the relative role of Nb and Pd and their possible location in the identified oxides. Because no M1 and/or M2 oxides could be identified, synergistic effects between nanocrystals of  $(\text{VMoNb})_5\text{O}_{14}$  and  $\text{V}_x\text{Mo}_{1-x}\text{O}_{3-0.5x}$  are proposed to account for the high catalytic performance of the multicomponent  $\text{MoVNb(Pd)}$ oxides.

## Keywords

**Ethane oxidation; acetic acid; ethylene; MoVNbO; Pd dopant; multicomponent catalyst; synergistic effect**

## 1. INTRODUCTION

The Mo-V-O system is the base of catalysts which are claimed by several companies to be active and selective in – at least – five oxidation reactions. Benzene to maleic anhydride [1] and acrolein to acrylic acid [2,3] are the oldest ones. Attempts to make value of ethane, which is available at low cost, then followed. The mild oxidation of ethane to ethylene and/or acetic acid on niobium-doped Mo-V-O was proposed in the open literature in 1978 by Thorsteinson et al. [4], and studied later on [5-11]. More recently, to the Mo-V-O system have been added several elements among which W, Nb, Sb and Te, which take part in the formation of crystalline structures. These multicomponent oxides have been studied for the (amm)oxidation of propane to acrylonitrile or acrylic acid [12-19]. Other catalysts based on vanadium were also proposed for C<sub>2</sub>H<sub>6</sub> [20-24] and C<sub>3</sub>H<sub>8</sub> [25,26] oxidations.

The tuning of Mo-V-O properties to fit one or the other reaction is a feature of this system which is versatile enough to incorporate other elements. The presence of these elements (whatever their nature and their content) is obviously a prominent factor, as it is responsible not only for the stabilisation of definite crystal structures, but also for the oxidation state of the component atoms at the steady state, in given operating conditions. Indeed, the reducing power of the gaseous mixture, and also the presence or absence of steam, strongly influence these characteristics. Restricting ourselves to Mo/V > 1:1 phases, several Mo-V-O compounds are known from literature [27,28]. The X-Ray diffraction pattern of some of them present the famous XRD line at  $d = 4.0 \text{ \AA}$  supposed to be related to selectivity to acrylic acid (from acrolein) [2, 3, 13], or to ethylene (from ethane) [4]. Depending on their structure, these Mo-V-O phases may, or may not, incorporate extra ions (dopants) in solid solution. Hexagonal bronze-type

precursors may be obtained as ammonium salts during preparation. Tungsten, niobium, aluminum, antimony, tellurium, etc., may partly replace molybdenum in Mo-O oxides, in the presence, or not, of vanadium. V-Sb-Al-O phases were first proposed to (amm)oxidize propane to (acrylonitrile) acrylic acid [25,26]. Higher yields being obtained with Mo-V-O doped with Nb and Te (or Sb), the latter system has been recently the subject of numerous investigations. Two multicomponent crystalline phases have been identified by several teams, beginning by Mitsubishi authors [14], which today are quite universally called M1 and M2 [29-33]. Promoters of Mo-V-O like Al, Ti, Fe, Cr, Ga were proposed by Ueda et al. [34] in amounts close to those of the propane (amm)oxidation catalysts, e.g.,  $\text{Mo}_6\text{V}_1\text{Al}_1\text{O}_x$ ,  $\text{Mo}_6\text{V}_2\text{Ga}_1\text{O}_x$ , and  $\text{Mo}_6\text{V}_3\text{Fe}_1\text{O}_x$ , respectively. The structures of M1 and M2 have been recently determined [30,33,35,36]. DeSanto et al. refined the M1 structure [35,36]. Its formula is  $\text{Mo}_{7.5}\text{V}_{1.5}\text{NbTeO}_{29}$  and its structure is orthorhombic, while that of  $\text{Mo}_6\text{Te}_2\text{VO}_{20}$  (M2) is hexagonal. Both X-ray diffraction (XRD) patterns exhibit a strong line at  $2\theta = 22.2^\circ$ . According to the most recent findings, a synergistic effect between M1 and M2 could be responsible for the high yields of acrylonitrile (59%) [37].

The catalytic performance of Mo-V-Nb-O phases were first examined in the oxidative dehydrogenation of ethane to ethylene by Thorsteinson et al. [4], who determined the optimum composition  $\text{Mo}_{0.73}\text{V}_{0.18}\text{Nb}_{0.9}\text{O}_x$ . Acetic acid was also formed but in small amounts and only at high pressure ( $P = 20$  bars). Analysis by XRD showed patterns typical of  $\text{V}_9\text{Mo}_6\text{O}_{40}$ -type oxides. Solids  $\text{Mo}_6\text{V}_3\text{Nb}_1\text{O}_x$  of stoichiometry close to  $\text{Mo}_{0.73}\text{V}_{0.18}\text{Nb}_{0.09}\text{O}_x$  with the same XRD pattern were also studied by Burch and Swarnakar [5], and later by Ruth et al. [7,8]. Other catalysts based on vanadium and able to form directly acetic acid were tested [6, 20-23]. Merzouki et al. [6,20] studied

the preparation of  $\text{Mo}_{0.73}\text{V}_{0.18}\text{Nb}_{0.09}\text{O}_x$  catalysts. The formation of acetic acid at low temperature ( $250^\circ\text{C}$ ) and atmospheric pressure was related to the presence of V,Nb-doped  $\text{Mo}_5\text{O}_{14}$  (besides  $\text{MoO}_3$ ). Instead of  $\text{V}_9\text{Mo}_6\text{O}_{40}$  (and/or  $\text{V}_6\text{Mo}_4\text{O}_{25}$ ) [4,5,7,8], the  $\text{Mo}_5\text{O}_{14}$ -type was obtained because of hydrochloric or oxalic acid added during preparation [6,20]. The authors suggested that molybdenum oxide was stabilised by means of microdomains of  $(\text{VNbMo})_5\text{O}_{14}$  [6], a hypothesis recently proposed in a study of  $\text{MoVO}_x$  and  $\text{MoVNbO}_x$  containing more vanadium [28]. More recently, the  $\text{MoV}_{0.25}\text{Nb}_{0.12}\text{O}_x$  catalyst doped with palladium has been the matter of a thorough structural and kinetic study for the same reaction [10,11], in which Pd was claimed to be responsible for the oxidation of ethylene to acetic acid in a Wacker-like process. Other recent and thorough studies were mostly devoted to the solid state chemistry of phases based on  $\text{Mo}_5\text{O}_{14}$  [17,18,38-41]. Among interesting results, the authors found a typical XRD pattern with a strongly amorphous character, similar to that of the MoVW catalyst claimed by BASF [13,18] to be active and selective for acrolein oxidation to acrylic acid. They have demonstrated that the XRD pattern fits well that of a mixture of nanocrystallites of  $(\text{VNbMo})_5\text{O}_{14}$  and of  $\text{MoO}_3$ . However in their recent papers the possibility that M1 or M2 phases could be present was not mentioned.

Although Te (Sb) does not seem to be the preferred dopant when one wants to oxidize ethane, the question as to whether channel structures like the one of M1 and/or M2 type phases may form without Te but in the presence of Nb is important. The role of Nb alone on  $\text{MoV}_{0.4}\text{O}_y$  properties has already been addressed in a former paper by Bouchard et al. [28] who used X-ray diffraction, laser Raman spectroscopy and X-ray photoelectron spectroscopies in normal and *in situ* conditions. We have decided to examine the influence of Nb and/or Pd dopants on the properties of  $\text{MoV}_{0.4}\text{O}_x$  system,

which is the basis of efficient catalysts for ethane oxidation to acetic acid and ethylene [9]. A catalyst without molybdenum but containing Nb and Pd was also prepared in order to compare with Mo-containing solids. The stoichiometry was kept constant, that is  $\text{Mo}_1\text{V}_{0.4}\text{Nb}_{0.12}\text{Pd}_{3.e-4}\text{O}_y$  when all atoms are present. Precursors were calcined at 350 and at 400°C, in order to examine the influence of calcination temperature on the phases present and on their catalytic properties. The physicochemical properties of catalysts and of the precursors obtained before calcination were also studied using several techniques and correlated with the catalytic performance.

## 2. EXPERIMENTAL

### 2.1. Preparation of Catalysts

Catalysts  $\text{MoV}_{0.4}\text{O}_x$  (MoV),  $\text{MoV}_{0.4}\text{Nb}_{0.12}\text{O}_x$  (MoVNb),  $\text{MoV}_{0.4}\text{Pd}_{3.e-4}\text{O}_x$  (MoVPd),  $\text{MoV}_{0.4}\text{Nb}_{0.12}\text{Pd}_{3.e-4}\text{O}_x$  (MoVNbPd), and  $\text{VNb}_{0.3}\text{Pd}_{3.e-4}\text{O}_x$  (VNbPd) were prepared according to Karim et al. [9] from ammonium heptamolybdate (AHM), ammonium metavanadate, niobium oxalate and palladium chloride aqueous solution. After desiccation of the mixture, the resulting powder was dried at 120°C overnight yielding the precursor P, which was then calcined in air up to  $T_c = 350^\circ\text{C}$  or  $400^\circ\text{C}$  (2 hrs). P- is preceding the label in the case of precursors (e.g., P-MoV for the precursor of  $\text{Mo}_1\text{V}_{0.4}$ ), while the temperature of calcination is written after the label, as in MoV-350 ( $\text{MoV}_{0.4}\text{O}_x$  calcined at  $T_c = 350^\circ\text{C}$ ).

## 2.2. Techniques of Characterisation

The specific surface area was determined by the B.E.T single point method. The range of surface areas was 15-35 m<sup>2</sup>/g. XRD patterns were acquired on Huber diffractometer using CuK $\alpha$  radiation. Lines were assigned to crystalline phases using the DIFFRACPlus software (Bruker) in the range  $2\theta = 3-60^\circ$ . Laser Raman spectra (LRS) were recorded using a Labram Infinity laser Raman spectrometer (JY-DILOR®) equipped with an optical microscope. The laser intensity (Ar<sup>+</sup>, 514.5 nm) was reduced by various filters (< 1 mW), and the data were treated by Labspec software. The spectral resolution and the accuracy of Raman shifts were evaluated at  $\sim 2\text{ cm}^{-1}$ . About ten particles of each sample were examined by optical microscopy to check their homogeneity. The reactivity of samples in air was qualitatively examined by submitting powder grains to the laser beam with the same following procedure. Filters of various powers (D3: 0.04; D2: 0.05; D1: 0.08; D0.6: 0.48 and D0: 0.67 mW) were used successively, the time of acquisition being different according to the filter (600, 540, 120 and 60 s for D3, D1, D0.6 and D0, respectively).

X-ray photoelectron spectroscopy (XPS) was performed using the VG-ESCALAB 220XL spectrometer. The powder samples were pressed in a 2 mm hole in a steel block. The Al K $\alpha$  monochromatized line (1486.6 eV) was used at 120 kV giving a 500  $\mu\text{m}$  spot diameter in the sample. The spectrometer was operated in a constant pass energy mode ( $E_{\text{pass}} = 30\text{ eV}$ ) for the high resolution spectra recording using the electromagnetic lens mode. There was no need of flood gun source as the samples were conducting enough. Binding energies were referenced to O 1s core (530.20 eV). During experiment the vacuum level was less than  $10^{-7}$  Pa. Experimental quantification level and spectral simulation were obtained using the Eclipse software provided by VG Scientific. The

area of Mo ( $3d_{3/2}$ ,  $3d_{5/2}$ ), V ( $2p_{3/2}$ ) and Nb ( $3d_{3/2}$ ,  $3d_{5/2}$ ) peaks was measured for each sample and the surface stoichiometry was determined. Signals were decomposed in order to get the relative amount of oxidized and reduced cations. The surface oxygen stoichiometry was then calculated and compared to the two extreme values obtained from bulk stoichiometry by considering cations in their oxidized or in their reduced forms, respectively.

### *2.3. Catalytic Testing*

The catalytic properties were measured using a conventional flow set-up, effluents being analyzed by on-line gas chromatography. The stainless-steel fixed bed reactor was placed in a tubular furnace and connected to the analysis set-up. The inlet gas mixture of propane, oxygen and nitrogen was controlled using mass flowmeters. The reactor (volume of catalyst = 3 mL) was fed with  $C_2H_6/O_2/N_2 = 40/6/54$  and operated at 240-280°C and contact time  $\tau = 1.2$  s. Reactants and products were analysed on-line with a gas chromatograph equipped with a double detector (thermal conductivity and flame ionization) and two columns, HayeSep D 80/100 mesh, and LAC446. In these conditions, the carbon balance was satisfied at  $\pm 2\%$ .

## **3- EXPERIMENTAL RESULTS**

### *3-1. Characterisation and Reactivity of Precursors*

XRD patterns of precursors obtained after drying show that several crystalline or poorly crystalline phases are present according to the presence (Nb series), or absence (Nb-free series) of niobium, the case of P-VNbPd being special. In the complex pattern

of Nb-free series precursors (P-MoV and P-MoVPd) (Fig. 1) are identified several Mo phases containing ammonium, among which ammonium heptamolybdate tetrahydrate (AHM) (JCPDS 70-1707),  $(\text{NH}_4)_2\text{Mo}_4\text{O}_{13}$  (JCPDS 80-0757) and  $(\text{NH}_4)_{0.2}\text{V}_{0.2}\text{Mo}_{0.8}\text{O}_3$  (JCPDS 73-0039). The intense line at  $8.3^\circ$  could not be attributed.  $(\text{NH}_4)_{0.2}\text{V}_{0.2}\text{Mo}_{0.8}\text{O}_3$  is isostructural to hexagonal molybdenum oxide h-MoO<sub>3</sub>, the structure of which is known to be stabilised by ammonium and/or protons [42,43]. The patterns of Nb-containing precursors present a markedly amorphous character (Fig. 2). In P-MoVNb, the two main lines centered at  $2\theta = 17.5^\circ$  and  $22.0\text{-}22.2^\circ$  may be assigned to  $\text{NH}_4\text{VO}_3$ , but also to  $\text{Mo}_5\text{O}_{14}$  (called  $\theta$ -phase) stabilised by V and/or Nb [44], respectively. Because it is impossible to check if V and/or Nb are, or not, inserted, the latter compound will thereafter be noted  $(\text{VNbMo})_5\text{O}_{14}$ . The main line in P-MoVNbPd at  $22.2^\circ$  and the broad line at  $25.5^\circ$  (corresponding to several lines) are also assigned to  $(\text{VNbMo})_5\text{O}_{14}$ . The pattern of P-VNbPd is different but it exhibits also a partly amorphous character, with few sharp lines belonging to ammonium vanadium oxides  $(\text{NH}_4)_x\text{V}_y\text{O}_z$ , among which  $\text{NH}_4\text{VO}_3$ , and to  $\text{V}_2\text{O}_5$ .

Few Raman reference spectra of the mixed Mo-V-O<sub>x</sub> phases have been recorded in literature [45], and none for precursors. The samples of the Nb-free series (P-MoV, P-MoVPd) are not homogeneous. For a dozen of particles selected under the microscope before acquisition of the spectrum, three types of pattern are obtained (Fig.3a, b, c). As expected, the spectrum of AHM (Fig. 3b) is the most common [46]. It consists in two broad intense lines at  $860$  and  $935\text{ cm}^{-1}$  and a wide weak band ca.  $1450\text{ cm}^{-1}$  assigned to  $\text{NH}_4^+$ . The two other spectra show that part of AHM has already been transformed into (mixed) oxides. Indeed, the pattern a) on Fig. 3 is made up of the main lines of orthorhombic  $\alpha\text{-MoO}_3$  ( $995, 820\text{ cm}^{-1}$ ),  $\text{V}_2\text{O}_5$  ( $995, 700\text{ cm}^{-1}$ ), ammonium metavanadate

(1437, 1416, 931, 498  $\text{cm}^{-1}$ ), and lines of h-MoO<sub>3</sub>-type with a weak band appearing *ca.* 1420  $\text{cm}^{-1}$ . That band is absent in the third type, c), of spectrum which is close to that of ‘disordered’  $\alpha$ -MoO<sub>3</sub> or of  $\alpha$ -V<sub>x</sub>Mo<sub>1-x</sub>O<sub>3-0.5x</sub> (*vide infra*) (Fig. 3c). On the contrary, all particles of Mo,Nb-containing precursors (P-MoVNb, P-MoVNbPd) display the same AHM-like spectrum (Fig. 3b). In first approximation, Nb could be responsible for a better homogeneity of the precursor material. Finally, the spectrum of P-VNbPd resembles that of NH<sub>4</sub>VO<sub>3</sub>. However the lines are broader, and the high intensity of NH<sub>4</sub><sup>+</sup> line (as compared to that in pure NH<sub>4</sub>VO<sub>3</sub>) could account for a strong perturbation of the lattice of NH<sub>4</sub>VO<sub>3</sub> by Nb.

The reactivity of the precursors was estimated by LRS by means of the heating action of the laser beam while changing the protective filter (Figs. 4, 5). In spectra of the Nb-free series (P-MoV and P-MoVPd), the formation of crystalline  $\alpha$ -MoO<sub>3</sub> (994, 820, 670, etc.,  $\text{cm}^{-1}$ ) is observed every time the AHM spectrum was initially exhibited. Laser heating provokes the decomposition of AHM as shown by the disappearance of the NH<sub>4</sub><sup>+</sup> bands. Bands at 980–850  $\text{cm}^{-1}$  may be characteristic of the intermediate hexagonal h-V<sub>x</sub>Mo<sub>1-x</sub>O<sub>3-0.5x</sub> mixed oxide ( $x = 0.12$ - $0.13$ ), which is finally decomposed into  $\alpha$ -MoO<sub>3</sub> (or  $\alpha$ -V<sub>x</sub>Mo<sub>1-x</sub>O<sub>3-0.5x</sub>), and probably V<sub>2</sub>O<sub>5</sub> (shoulder at 700  $\text{cm}^{-1}$ ) (Fig. 4). In the case of P-MoVPd exhibiting disordered  $\alpha$ -MoO<sub>3</sub> spectrum, lines at 1100, 790 and 560  $\text{cm}^{-1}$  after heating are characteristic of silicates and assigned to the glass holder. The examined particles had therefore been volatilized, as it also happens with P-VNbPd samples. Therefore, the presence of Pd is assumed to be responsible for less stability of these Nb-free materials during laser heating.

On the contrary, in Nb series, the heating of P-MoVNb particles constituted of AHM (Fig. 5) gives mostly rise to  $\alpha$ -MoO<sub>3</sub> (990, 820, 667, 285  $\text{cm}^{-1}$ ) and to some (disordered)

$V_2O_5$  (shoulder at 985 and broad band *ca.* 700  $cm^{-1}$ ). In the presence of Pd (P-MoVNbPd), at first AHM gives rise to  $\alpha$ - $MoO_3$  (995  $cm^{-1}$ ) and  $V_2O_5$  (700 and 290  $cm^{-1}$ ), while lines at 960-850  $cm^{-1}$  are assigned to hexagonal  $V_xMo_{1-x}O_{3-0.5x}$  which remains stable up to the last change. Among lines of disordered  $\alpha$ - $MoO_3$  (or  $\alpha$ - $V_xMo_{1-x}O_{3-0.5x}$ ) and  $V_2O_5$  (700  $cm^{-1}$ ), a small massif centered at 900  $cm^{-1}$  is retained which remembers that found in LRS of  $Mo_5O_{14}$ -type oxides [45].

### 3-2. Characterisation of Catalysts Calcined at 350 and 400°C

#### X-Ray Diffraction

Two main types of diffraction pattern are observed according to the composition of catalysts (Figs. 6, 7, Table 1): (i) numerous lines for Nb-free crystalline solids, (ii) an almost amorphous pattern for Nb-containing solids, to which are superposed several lines in the cases of MoVNb-400 and of VNbPd. Lines of crystalline  $\alpha$ - $MoO_3$  are often observed, particularly when samples were calcined at 400°C. A feature common to all Mo-containing catalysts is the presence of a line at  $d(\text{Å})/2\theta^\circ = 4.0 / 22.2$ .

Besides  $\alpha$ - $MoO_3$ , several phases can be identified in Nb-free samples calcined at 350 and 400°C (MoV and MoVPd) (Figs. 6, 7). The fact that most lines of  $\alpha$ - $MoO_3$  are shifted as compared to the standard pattern (JCPDS 76-1003) may be assigned to a modification by vanadium (e.g. orthorhombic  $\alpha$ - $V_xMo_{1-x}O_{3-0.5x}$ ) or to the formation of oxygen vacancies, as in  $MoO_{3-x}$ . The presence of  $Mo_5O_{14}$ -type structure is ascertained by the strongest reflections at  $d(\text{Å})/2\theta^\circ = 3.99/22.2$  and  $3.56/24.94$ , and by two medium lines at  $11.4/7.74$  and  $10.2/8.67$  (JCPDS 31-1437). These lines are absent in MoV400 pattern. Triclinic  $V_{0.95}Mo_{0.97}O_5$  (JCPDS 77-0649), the pattern of which is very close to

that proposed for  $\text{VMo}_3\text{O}_{11}$  [2, 3], is characterised, among others, by a line at  $2\theta \sim 22.0^\circ$  that cannot be mistaken with the one at  $22.2^\circ$  of  $\text{Mo}_5\text{O}_{14}$ -type. In MoV-350 pattern, a fourth phase is related to the hexagonal defective h- $\text{MoO}_3$  oxide, its XRD lines fitting as well those of  $\text{V}_{0.12}\text{Mo}_{0.88}\text{O}_{2.94}$  (JCPDS 81-2414). These lines are not present in MoV-400 pattern because of the poor stability of these h- $\text{MoO}_3$ -type phases which are transformed into  $\alpha$ - $\text{MoO}_3$  or isostructural orthorhombic  $\alpha$ - $\text{V}_x\text{Mo}_{1-x}\text{O}_{3-0.5x}$  above  $350^\circ\text{C}$ . The lines of  $\alpha$ - $\text{MoO}_3$ -type are indeed more intense, as they are in the case of MoVPd-400.

The pattern of Nb-containing catalysts exhibits an amorphous character. For MoVNb-350 and MoVNbPd-350 (Fig. 6), several very broad reflections at  $2\theta \sim 12.5^\circ$  and  $\sim 27^\circ$  have been assigned to particles of  $\alpha$ - $\text{MoO}_3$  by Mestl et al. [38] who emphasized the nanocrystalline character of that material. Lines at  $2\theta^\circ \sim 7.8, 8.7$  and  $22.2$  (the most intense) correspond to (200), (210) and (001) planes and are characteristic of  $\theta$ - $\text{Mo}_5\text{O}_{14}$  structure [44]. The pattern of  $\text{Nb}_2\text{Mo}_3\text{O}_{11}$  (JCPDS 18-0840) shows intense reflections at  $d(\text{\AA})/2\theta = 10.92/8.08^\circ$  and  $4.00/22.2^\circ$ . It is very close to that of  $(\text{Nb}_{0.09}\text{Mo}_{0.91})\text{O}_{2.80}$  (JCPDS 27-1310) but the latter formula fits better our Nb/Mo = 0.12 stoichiometry. Because of the amorphous character of the pattern, it is not possible to choose between  $(\text{V}_{0.07}\text{Mo}_{0.93})_5\text{O}_{14}$  (JCPDS 31-1437),  $(\text{Nb}_{0.09}\text{Mo}_{0.91})_5\text{O}_{14}$  (JCPDS 27-1310), or a ternary solid solution  $(\text{V}_x\text{Nb}_y\text{Mo}_{1-x-y})_5\text{O}_{14}$ . The pattern of MoVNb-400 (Fig. 7) exhibits the main lines of  $\alpha$ - $\text{MoO}_3$  (or of  $\alpha$ - $\text{V}_x\text{Mo}_{1-x}\text{O}_{3-0.5x}$ ) superposed to the preceding pattern. This indicates that the  $\alpha$ - $\text{MoO}_3$ -type nanoparticles, already present at  $T_c = 350^\circ\text{C}$ , have partly grown as bigger crystals. However, the pattern of MoVNbPd-

400 does not exhibit these lines. The stabilisation of  $\alpha$ - $\text{MoO}_3$ -type nanoparticles may be considered as an indirect proof of the incorporation of vanadium (*vide infra*).

The XRD patterns of VNbPd-350 and VNbPd-400 (Table 1) exhibit lines characteristic of  $\text{V}_2\text{O}_5$  and of  $\text{NbVO}_5$  [5, 47, 48], the strongest reflection of the latter being at  $2\theta = 21.92^\circ$ . The crystalline state is improved when  $T_c = 400^\circ\text{C}$  (VNbPd-400). A feature common to MoVNb catalysts is the amorphous character of the XRD pattern of VNbPd-350, meaning that Nb is responsible for the formation of small and disordered particles.

#### *Laser Raman Spectroscopy*

The Raman spectra of Mo-containing catalysts calcined at  $350^\circ\text{C}$  (Fig. 8) are almost the same (Table 1). They are characterized by an intense triplet in  $950\text{-}820\text{ cm}^{-1}$  range, and a wide medium massif centered *ca.*  $700\text{ cm}^{-1}$ . Slight differences seem to be related to the presence/absence of Nb. In Nb-free samples, some lines assigned to  $\alpha$ - $\text{MoO}_3$  (particularly the vibration of Mo-O-Mo and Mo=O bonds at  $818$  and  $994\text{ cm}^{-1}$ , respectively) are more (MoV-350) or less (MoVPd-350) intense (Fig. 8). The triplet, which is observed at  $925$ ,  $890$  and  $845\text{ cm}^{-1}$  in MoV-350, is shifted to  $928$ ,  $872$ ,  $830\text{ cm}^{-1}$  in MoVNbPd. Generally, Raman lines at  $860\text{-}940\text{ cm}^{-1}$  are assigned to the M-O-M' stretching mode of polycrystalline  $\text{MM}'\text{O}$  mixed metal oxides, while those *ca.*  $1000\text{ cm}^{-1}$  are assigned to the M=O (or M'=O) stretching mode. More particularly, lines at  $932$  and  $873\text{ cm}^{-1}$  are related to Mo-O-V phases. In their study of Mo-V-O system doped with tungsten, Mestl et al.[45] assigned lines at  $940\text{-}860\text{ cm}^{-1}$  and massif *ca.*  $700\text{ cm}^{-1}$  to a 'nanocrystalline'  $\text{Mo}_5\text{O}_{14}$ -type mixed oxide with partial substitution of Mo by V and/or W. Indeed, as niobium, tungsten also affects the crystallinity of Mo-mixed

oxide [39]. Therefore, our MoV and MoVPd samples do contain  $(\text{VMo})_5\text{O}_{14}$  while nanocrystalline MoVNb and MoVNbPd do contain  $(\text{VNbMo})_5\text{O}_{14}$ , in accordance with XRD patterns. However, the question as to whether hexagonal mixed oxides could also be present in samples calcined at 350°C cannot easily be answered, because their main lines are located in the same range. A noticeable difference exists between Nb-containing and Nb-free samples calcined at 400°C (Fig. 9). In the LRS spectrum of the former, the characteristic lines of nanocrystalline  $\text{Mo}_5\text{O}_{14}$ -type are still present (950-820 and 700  $\text{cm}^{-1}$ ), whereas in Nb-free catalysts either they have completely disappeared, or their intensity has considerably decreased. The latter modification occurs simultaneously with a relatively strong increase of the intensity of  $\alpha$ - $\text{MoO}_3$ -type lines.

A completely different spectrum is exhibited by Mo-free samples (Table 1). Whatever  $T_c$ , the spectrum of VNbPd exhibits lines at 993, 700, 526, 482, 405, 304, 282, 200 and 146  $\text{cm}^{-1}$  which are characteristic of crystalline  $\text{V}_2\text{O}_5$ . The presence of  $\text{VNbO}_5$  detected by XRD could be accounted for by the weak shoulder at ca. 970  $\text{cm}^{-1}$ , but other lines at 740, 310 and 220  $\text{cm}^{-1}$  said to be characteristic [49] could not be observed.

#### *X-Ray Photoelectron Spectroscopy*

The binding energies of Mo  $3d_{5/2}$ , V  $2p_{3/2}$  and Nb  $3d_{5/2}$  for catalysts calcined at 350 and 400°C are reported in Table 2. In the literature, the ‘standard’ values are  $232.4 \pm 0.2$  for  $\text{Mo}^{6+}$ ,  $516.6 \pm 0.1$  for  $\text{V}^{5+}$ ,  $515.9 \pm 0.4$  for  $\text{V}^{4+}$  and  $207.4 \pm 0.9$  eV for  $\text{Nb}^{5+}$  [50-54]. In our samples, the Mo photopeak is characteristic of  $\text{Mo}^{6+}$  by its BE as well as by its FWHM. Reduced Mo specie as  $\text{Mo}^{5+}$  (230.8-231.8 eV) or  $\text{Mo}^{4+}$  [50,51] are absent, while on the contrary part of vanadium is reduced. The relative amounts of  $\text{V}^{5+}$  and  $\text{V}^{4+}$  are reported in Table 3 after peak decomposition. Niobium remains as  $\text{Nb}^{5+}$  because its

Nb  $3d_{5/2}$  BE is higher than 205.2–206.1 eV as recorded for Nb<sup>4+</sup> [50]. Palladium was not searched for because of its very low concentration.

The comparison of atomic ratios along the Mo catalyst series ( $T_c = 350^\circ\text{C}$ ) reveals the influence of Pd and/or Nb on surface composition. Pd addition to MoV ( $V/\text{Mo} = 0.40$  to  $0.36$ ), or to MoVNb ( $V/\text{Mo} = 0.50$  to  $0.43$ ), results in an increase of the amount of surface vanadium (or a decrease of the amount of surface Mo). The same observation applies when adding Nb to MoV ( $0.43$  to  $0.36$ ) or to MoVPd ( $0.50$  to  $0.40$ ). In other words, both Nb and Pd dopants contribute to stabilise part of molybdenum in the bulk, since the Nb/Mo ratio does not change much (although it is lower than for fresh catalysts). The amount of oxygen determined from surface composition is lower than when it is calculated from bulk stoichiometry (all V assumed to be V<sup>4+</sup>) in only two cases: MoV-350 and MoVPd-350. It means that a small amount of reduced specie (Mo<sup>5+</sup>, V<sup>3+</sup>) could be present.

The  $V^{5+}/V^{5+}+V^{4+}$  ratio ranges from 0.76-0.80 (MoVNbPd-350, MoVPd-350) to 0.81-0.83 (MoVNb-350, MoV-350) (Table 3), which shows that both Pd and Nb increase the reducibility of vanadium. When catalysts are calcined at  $400^\circ\text{C}$ , this ratio is generally lower. Because this means that the reducibility has increased, it may be that less vanadium is inserted in the mixed Mo(Nb) phase(s). The effect of vacuum in XPS apparatus is also known to provoke the reduction of some V<sup>5+</sup> [55], but this happens only if these ions are not properly stabilized in an oxide matrix. The Nb/Mo values do not change much and they are similar to those at  $T_c = 350^\circ\text{C}$ . A part of Nb is therefore located inside the bulk.

The spectrum of VNbPd is different from those of Mo-containing catalysts. There is more Nb on the surface as compared to the bulk ( $V/\text{Nb} \sim 2.06$  vs.  $3.2$ ). Table 3 shows

no difference of oxygen stoichiometry when  $T_c$  changes. The relative amount of  $V^{4+}$  is smaller (13-15%) as compared to 17-30% in Mo-based catalysts, which means that the vanadium is less reducible in the presence of niobium (and Pd) than in the presence of Mo.

### 3-3. Catalytic properties

The products obtained by oxidation of ethane are mainly ethylene and acetic acid, and carbon oxides. Very little acetaldehyde and formaldehyde are formed (less than 1 mol%). Experiments were carried out so as to maintain oxygen that is not fully converted. In these operating conditions, the maximum conversion ( $X$ ) of ethane to acetic acid (AA) and ethylene (EE) (at 100 mol% selectivity) is 10 and 30 mol%, respectively.

When examining the activity of catalysts calcined at 350°C by varying the reaction temperature  $T_R$  between 240 and 280°C, two series are noted: MoVPd and VNbPd are poorly active ( $X_{max} = 4$  mol%), whereas the conversion varies strongly upon increasing  $T_R$  by only 40°C ( $X_{max} = 13.8$  mol%) with MoV-350 and MoVNb-350 (Fig. 10). The selectivity to carbon oxides as compared to the total selectivity ( $S_{AA} + S_{EE}$ ) to mild oxidation products is higher for those catalysts, MoVPd and VNbPd, which are poorly active. The formation of carbon monoxide compared to that of  $CO_2$  is also informative. The  $S_{CO}/S_{CO+CO_2}$  amounts to 0.3-0.1 for the latter and 0.6-0.5 mol% for MoV-350 and MoVNb-350. Catalysts calcined at 400°C are less active, particularly MoV-400. The two categories remain when comparing selectivities to ethylene and acetic acid (Figs 11, 12). The highest selectivity to ethylene (70-55 mol%) is obtained with MoV-350 and MoVNb-350, while it is very low for MoVPd-350 and VNbPd-350 (9-0 mol%). These

values are not much modified for catalysts calcined at 400°C, except for MoV-400 in which case the CO<sub>x</sub> production increases strongly. Acetic acid follows the reverse trend. S<sub>AA</sub> is high for MoVPd-350 (72-65 mol%), and for VNbPd-350 at T<sub>R</sub> = 240°C only, while S<sub>AA</sub> ≈ 30 mol% for MoV-350 and MoVNb-350. To summarize, the increase of T<sub>c</sub> from 350 to 400°C results in an increase of CO<sub>x</sub> at the expense of both acetic acid and ethylene. Whereas MoV catalyst experiences the strongest variations, the catalytic performance of MoVNb remains quite constant. The difference of activity of all catalysts calcined at 350°C becomes striking when selectivities are plotted against conversion (Fig. 13). Their performance can be compared at low isoconversion only. E.g., at X = 3.5 mol%, S<sub>AA</sub> decreases along MoVPd (58) > MoV = MoVNb (28 mol%) = VNbPd, and S<sub>EE</sub> decreases along MoVNb (72) > MoV (65) >> MoVPd (5) = VNbPd (3 mol%). A high total selectivity to acetic acid and ethylene is obtained only with MoV and MoVNb catalysts, in which cases the selectivity to CO<sub>x</sub> is as low as 7-13 and 3.8-7 mol%, respectively. In the same conditions, a sample of MoVNbPd-350 catalyst gives S<sub>AA</sub> = 45.5 and S<sub>EE</sub> = 42.5, respectively, at X = 6.0 mol%.

#### 4- DISCUSSION

Several parameters influence the physicochemical as well as the catalytic properties of the mixed oxides. The nature and crystallinity of phases and the surface composition of the fresh catalysts depend on T<sub>c</sub>, the temperature of calcination. Because the whole chemical analyses show that the presence of Nb and/or Pd in the solids is a determining factor even at the precursor stage, the discussion will be led by considering the Nb-free (MoV, MoVPd) or Nb-containing (MoVNb, MoVNbPd) series. VNbPd catalysts belong to one or the other series, depending on the examined properties.

### *Precursors: Influence of Nb and of Pd*

After drying, phases in the precursors are mostly crystalline in the Nb-free series (P-MoV and P-MoVPd) or mostly amorphous (P-MoVNb, P-MoVNbPd and P-VNbPd) in the presence of Nb (Figs. 1, 2). In the particles of Nb-free precursors, some unreacted ammonium heptamolybdate remains but part of it has been already transformed during the heating of solution and/or desiccation and drying. Indeed, other ammonium salts like  $(\text{NH}_4)_2\text{Mo}_4\text{O}_{13}$  and hexagonal ammonium and/or protonic bronzes like  $(\text{NH}_4)_{0.2}\text{V}_{0.2}\text{Mo}_{0.8}\text{O}_3$  or  $\text{H}_x\text{V}_x\text{Mo}_{1-x}\text{O}_3$  are particularly well identified by XRD. Micro Raman spectroscopy shows that Nb-free particles are not homogeneous, since several phases are present:  $\alpha\text{-MoO}_3$ ,  $\text{V}_2\text{O}_5$ , and  $\text{NH}_4\text{VO}_3$  or  $(\text{NH}_4)_x\text{H}_y(\text{Mo},\text{V})_z\text{O}_p$  bronze, are identified. XRD shows that in the Nb-containing series, the  $\theta$ -phase  $(\text{VMoNb})_5\text{O}_{14}$  has already been formed, even at room temperature. Although it is probable, the insertion of V and/or Nb at this stage cannot be directly checked because the XRD linewidth is too large. LRS reveals the presence of AHM in the 1  $\mu\text{m}$  depth of all particles analysed, the two lines of which (860 and 935  $\text{cm}^{-1}$ ) appear in the same range than those of  $\theta$ -phase (830, 870, 928  $\text{cm}^{-1}$ ) (Figs. 3b and 8). One must also remember the high Raman scattering cross section of molybdenum [56] which may mask lines of V (Nb) oxides. Indeed, lines of ammonium metavanadate were more intense in the spectrum of the Mo-free P-VNbPd.

When examined under laser beam heating, the reactivity of precursors again depends on the presence of Mo, Nb or Pd (Figs. 4,5). The formation of  $\alpha\text{-MoO}_3$  is observed at the end of experiments everytime AHM was identified in a precursor spectrum (Nb-free: P-MoV and P-MoVPd). Hexagonal ammonium-proton bronzes give rise to hexagonal mixed V,Mo oxides which are finally decomposed into  $\alpha\text{-MoO}_3$  or  $\alpha\text{-$

$V_xMo_{1-x}O_{3-0.5x}$ , and probably into  $V_2O_5$ , particularly in Pd-containing precursors (P-MoVPd and P-VNbPd). Palladium can be said to favor the instability of the materials because the spectrum of the glass holder is finally recovered after volatilization of the material. However, Nb-containing precursors (P-MoVNb and P-MoVNbPd) behave differently. Besides  $\alpha$ - $MoO_3$  (probably V-doped) and  $V_2O_5$  which are generally observed, hexagonal mixed oxides like  $(V_{0.12}Mo_{0.88})O_{2.94}$  or  $(V_{0.13}Mo_{0.87})O_{2.925}$  remain stable. Therefore, apart from the fact that the Nb to Pd atomic ratio is very high, their respective role is different. Niobium is responsible for a textural effect consisting in a partial amorphization of the  $(MoV)O_x$  solids which is related to the nanosized particles. Palladium is responsible for the instability of precursors in the absence of Nb, if it is not properly accommodated in the oxidic network.

*Catalysts: Influence of  $T_c$  and of Pd in Nb-free catalysts*

During calcination of the precursors up to 350 or 400°C, the remaining oxalate and ammonium groups are eliminated as  $CO_2$  and  $NH_3$  and/or  $NO$ , depending on the atmosphere, heating rate, and precursor type. In particular, it is well-known that the oxidation of  $NH_3$  to  $NO_x$  proceeds because vanadium and/or molybdenum undergo reduction. In air, pure unreacted AHM particles are first transformed into h- $MoO_3$  (providing the rate of heating is slow enough and  $T_c \leq 350^\circ C$ ) and then to orthorhombic  $\alpha$ - $MoO_3$  ( $T_c = 400^\circ C$ ). The structure of h- $MoO_3$  is depicted as double chains of face-sharing  $MoO_6$  octahedra arranging channels along c axis in which alkaline ions and/or protons are displayed. Compositions are  $A_{6x}([\square_x]Mo_{6-x})O_{18}$  ( $\square$  = Mo vacancy; A = Na- $2H_2O$ , K,  $NH_4$ , Rb, Cs, etc.). In the presence of vanadium, mixed (hydrated) hexagonal oxides isotypic to h- $MoO_3$ , like  $A_xV_xMo_{1-x}O_3$  ( $x = 0.13-0.20$ ) and  $H_xV_xMo_{1-x}O_3$  ( $0.06 \leq x \leq 0.18$ ), have also been synthesized [42,43]. These phases are stable as long as

ammonium (or alkaline cations) and/or protons remain located in the channels.

According to Dupont et al. [42], the heating of  $\text{H}_{0.13}\text{V}_{0.13}\text{Mo}_{0.87}\text{O}_3$  in air at  $350^\circ\text{C}$  leads to the formation of hexagonal  $(\text{V}_{0.13}\text{Mo}_{0.87})\text{O}_{2.935}$ , which is stable up to  $460^\circ\text{C}$ , contrary to V-free hexagonal bronzes. Moreover, the authors showed that, above this temperature, this solid is irreversibly transformed into a stable orthorhombic mixed oxide, isotypic to  $\alpha\text{-MoO}_3$ , which retains the same  $\text{V}/\text{Mo} = 0.13/0.87$  ratio. Therefore when calcined at  $T_c = 400^\circ\text{C}$ , these Mo,V mixed phases could be transformed into orthorhombic  $\text{V}_{0.13}\text{Mo}_{0.87}\text{O}_{2.925}$ . The free diameter of channels in the structure of  $\text{H}_{0.13}\text{V}_{0.13}\text{Mo}_{0.87}\text{O}_3$  or of hexagonal  $\text{V}_{0.13}\text{Mo}_{0.87}\text{O}_{2.935}$  is large enough ( $\approx 3.5 \text{ \AA}$ ) to accommodate  $\text{Pd}^{2+}$  ( $r = 0.86 \text{ \AA}$  for 6-coordination) [57] (Table 4). The study of the reactivity of P-MoVPd shows that this hypothesis is unlikely for this material. Indeed, the hexagonal phase could not be identified by XRD or LRS in MoVPd-400, the reason being that the presence of Pd quickens its decomposition. The  $\theta\text{-(VMo)}_5\text{O}_{14}$  phase has also been identified in Nb-free samples calcined at  $350^\circ\text{C}$  (XRD, LRS), but in lower amounts, and in a higher crystalline state, than in Nb-containing catalysts. By calcination at  $400^\circ\text{C}$ , the  $\alpha\text{-MoO}_3$  (or  $\alpha\text{-V}_{0.13}\text{Mo}_{0.87}\text{O}_{2.925}$ ) nanoparticles observed after calcination at  $350^\circ\text{C}$  have grown. Again, when it is present, palladium quickens this recrystallization. In their study of Pd-doped VPO catalyst, Merzouki et al. [20] demonstrated that Pd acts as a catalyst of the  $\text{V}^{5+}/\text{V}^{4+}$  redox system, but that if  $\text{Pd}^{2+}$  is not properly stabilized, its effect (or that of metallic Pd) may be detrimental to the formation of acetic acid. In our samples, the valence state and the exact location of Pd cannot be determined. In the case of MoVPd the trend of vanadium is to migrate towards the surface when  $T_c$  increases. As no vanadium oxide but molybdenum oxide

could be detected (XRD, LRS), this points out in turn the state and location of vanadium, that will be discussed later.

The catalytic performance of the 'Nb-free' catalysts, which includes MoV-400 (but not MoV-350), MoVPd, and also VNbPd (whatever  $T_c$ ), is characterized by a low activity in the studied operating conditions. The range of conversions of ethane is narrower for MoVPd and VNbPd ( $X = 1.0$  to  $4.4$  mol%, depending on  $T_c$ ) than for the Nb-containing series ( $X = 1.5$ - $13.5$  mol%). Nb-free catalysts are more selective to acetic acid than to ethylene. The selectivity to ethylene is essentially zero in the absence of Mo (VNbPd).  $S_{AA}$  is about 2.5 times higher (at low conversion) with MoVPd-350 than with MoV350. Yields to AA are 0.87-2.2 for MoVPd and 0.7-1.5 for VNbPd, compared to 0.9-3.3 mol% for MoV-350. These catalysts have also a high proportion of vanadium on their surface as compared to the bulk, as shown by XPS. Therefore, a high selectivity to acetic acid could be related to a high number of surface vanadium sites. However, these poorly active catalysts give more combustion products and proportionally less CO than Nb-containing catalysts ( $S_{CO}/S_{CO_x} = 0.0$ - $0.4$  instead of  $0.5$ - $0.6$ ). If some (or all) Pd is not stabilized as  $Pd^{2+}$  inside a given oxidic phase, the lesser amount of CO could be related to the presence of some metallic palladium, which is well known for its high activity in the combustion of CO, even at low temperature.

#### *Influence of $T_c$ and of Pd in Nb-Containing Catalysts.*

The amorphous character of Nb-containing catalysts (except VNbPd) makes it difficult to propose an accurate description of these Nb-containing catalysts. Hexagonal mixed oxides like  $V_xMo_{1-x}O_{3-x/2}$  and tetragonal  $\theta$ -(VNbMo) $_5O_{14}$  cannot be distinguished by XRD (most of their main XRD lines lie in the same  $2\theta$ -range), nor by LRS (Mo-O-V vibrations give rise to similar massif than Mo-O-Mo in the same range of

wavenumbers). Following Merzouki et al. [6] and Mestl et al. [38], we assume that MoVNb and MoVNbPd catalysts are composed of  $\theta$ -(VMoNb)<sub>5</sub>O<sub>14</sub> and  $\alpha$ -MoO<sub>3</sub> nanoparticles, although part of the excess of V is certainly accommodated as  $\alpha$ -V<sub>x</sub>Mo<sub>1-x</sub>O<sub>3-x/2</sub>. Indeed, the  $\theta$ -phase accounts for the similarity between MoVNb catalysts and the industrial MoVW catalyst of acrolein oxidation [8,13], because W, like V and Nb, is known to stabilize the  $\theta$ -oxide [44]. The framework of  $\theta$ -Mo<sub>5</sub>O<sub>14</sub> contains MoO<sub>7</sub> pentagonal bipyramids, the equatorial edges of which are shared with five MoO<sub>6</sub> distorted octahedra ([MoO<sub>7</sub>]5MoO<sub>6</sub> clusters). This pattern is isolated from the three others by corner-shared MoO<sub>6</sub> octahedra. Vanadium (as V<sup>4+</sup>) is supposed to replace Mo in octahedra, while Nb<sup>5+</sup>, whose size is large enough to be 7-coordinated (ionic radius  $r = 0.73 \text{ \AA}$ ) (Table 4), may be located in pentagonal bipyramids. In this way, there is no need to consider Mo<sup>4+</sup> ions ( $r = 0.65 \text{ \AA}$ ) which are known to be detrimental to catalytic activity. The large width of the (001) line of  $\theta$ -(VMoNb)<sub>5</sub>O<sub>14</sub> nanocrystals accounts for a high degree of disorder in the stacking of (001) planes, which could be provoked by the insertion of V, Nb. The same interpretation may be proposed for V in the case of stacked (010) planes of orthorhombic  $\alpha$ -V<sub>x</sub>Mo<sub>1-x</sub>O<sub>3-x/2</sub>.

The growing of  $\alpha$ -MoO<sub>3</sub> ( $\alpha$ -V<sub>x</sub>Mo<sub>1-x</sub>O<sub>3-x/2</sub>) particles when  $T_c = 400^\circ\text{C}$  (Nb-free series) is not observed for Nb-containing catalysts (MoVNb-400 and MoVNbPd-400). It means that these crystals are stabilised in their nanometer size, which is another (indirect) evidence of the insertion of V in  $\theta$ -(VMoNb)<sub>5</sub>O<sub>14</sub> and in V<sub>x</sub>Mo<sub>1-x</sub>O<sub>3-0.5x</sub>. During the *in situ* XRD reduction of MoVNb-350 by H<sub>2</sub>, the formation of a V<sub>x</sub>Mo<sub>1-x</sub>O<sub>2</sub> solid solution could be observed by Bouchard et al. [28], while MoO<sub>2</sub> only was identified in MoV-350. For a reason which is not yet known, it seems that Nb promotes the formation of solid solutions of (V,Mo)O<sub>x</sub>, probably as early as the stage of

preparation, as inferred from LRS experiments. Formerly, we had attempted to explain this stabilisation by considering the formation and ‘isolation’ [58] of the  $[\text{MoO}_7]_5\text{MoO}_6$  clusters of  $\theta\text{-(VMoNb)}_5\text{O}_{14}$  coherently grown in a matrix of (010)  $\alpha\text{-MoO}_3$  [6,28,58,59-61]. This model fits well the findings of Werner et al. [17] on  $\text{Mo}_4\text{VO}_{14}$ , which is isostructural to  $\theta$ -oxides. Using high resolution transmission electron microscopy, the authors showed that “a continuum random network of basic structural units (distorted octahedra) was detected made up of approximately circular clusters embedded in a quadratic network”. However, the surface composition of several MoV catalysts of different compositions (whatever  $T_c$ ) does not show an excess of Mo (except for MoV-350), but most often it shows a slight excess of V (except in the case of MoVNbPd), as compared to bulk stoichiometry. Let us recall that the crystal structure of  $\text{V}_2\text{O}_5$  and related  $\text{V}_n\text{O}_{2n+1}$  suboxides is very close to that of  $\alpha\text{-MoO}_3$  (and thus of  $\text{V}_{0.13}\text{Mo}_{0.87}\text{O}_{2.935}$ ): a similar framework (corner-sharing and/or edge-sharing octahedra) and the same mean size of octahedra. This is the reason why so many mixed oxides exist in the V-Mo-O system [62]. Therefore, layers or intergrowths of  $\text{VO}_x$  with the  $\theta$ -oxide (or part of its framework) could be as well considered.

Finally, the relative role of Nb and Pd is worthwhile to compare.  $\text{Nb}^{5+}$  is an early transition metal cation which behaves similarly to V and Mo cations (in their highest oxidation states), except that it is less reducible. Like  $\text{V}_2\text{O}_5$ ,  $\text{MoO}_3$ , etc., the structure of its various oxides is related to that of  $\text{ReO}_3$ . On the contrary,  $\text{Pd}^{2+}$  is a large cation often square-coordinated but which also accepts to be 6-coordinated (Table 4). Moreover, oxides of early transition metal cations are far more acidic than PdO, as shown when the scale of ‘optical basicity’,  $\Lambda$ , is used [63,64]. The optical basicity takes into account not only the type (ionic to covalent) of the M-O bond but also the extent (through

polarizability) of the negative charge borne by oxygen linked to the metallic cation. A scale of this acidity vs. the same  $O^{2-}$  base enables one to rank cations by means of their  $\Lambda$  value which depends on their valence, coordination and spin in the considered oxides. When comparing the optical basicity for the same 6-coordination,  $\Lambda = 0.61$  for  $Nb^{5+}$  is close to that of  $V^{5+}$  ( $\Lambda = 0.63$ ) or  $V^{4+}$  ( $\Lambda = 0.68$ ), while  $Mo^{6+}$  ( $\Lambda = 0.52$ ) and  $W^{6+}$  ( $\Lambda = 0.51$ ) (all hexacoordinated) are slightly more acidic (Table 4). On the contrary,  $Pd^{2+}$  is a soft cation, more basic than the early transition metal cations ( $\Lambda = 1.11$ ). Nevertheless, the question of the location of Pd is raised. Linke et al. [10] observed that the surface composition of their  $MoV_{0.25}Nb_{0.12}Pd_{5e-4}O_x$  catalyst was enriched with Pd after catalytic experiments, and proposed that the  $\theta$ -phase could serve as a host structure. Indeed, this structure contains hexagonal channels which are (theoretically) large enough (diameter  $\sim 2.15 \text{ \AA}$ ) to accommodate palladium as  $Pd^{2+}$ . However Pd could be also associated with the surface vanadium oxide phase, in a similar interaction as that the one proposed by Seoane et al. [65] for  $V_2O_5$ , or by Merzouki et al. [20] for V-P-O. In these two cases, Pd was shown to accelerate the rate of the  $V^{5+} + e \leftrightarrow V^{4+}$  redox. Moreover, in the first case ( $V_2O_5$ ) the formation of a specific suboxide,  $V_4O_9$ , was observed instead of  $VO_2$  [65]. As both crystal structures of  $VOPO_4/(VO)_2P_2O_7$  [66,67] and  $V_2O_5$  have a layered character, but no room to accommodate  $Pd^{2+}$  which is too big, the only way for Pd to be stabilised is to be trapped in between the layers. Obviously, in such a case the stabilisation of  $Pd^{2+}$  is poor, particularly in a reducing atmosphere. Comparatively, if  $Pd^{2+}$  can be accommodated in the channels of  $(VMoNb)_5O_{14}$  structure, its stabilisation is expected to be stronger.

From the catalytic performance point of view, MoV-350 and MoVNb-350 behave similarly. They give the same high selectivity to ethylene, which has been attributed to

the presence of the  $\theta$ -oxide [28]. These catalysts are more active and more selective to mild oxidation products (AA + EE) than MoVPd and VNbPd. The conversion of ethane varies by a factor of 2 to 3, the selectivity is lower to acetic acid than to ethylene ( $S_{AA}/S_{AA+EE} \sim 0.3$ ), and the selectivity to  $CO_x$  is about 4-15% that of the total selectivity  $S_{AA+EE}$ . The comparison to the catalytic performance of VNbPd is fruitful. The direct contribution of  $Nb^{5+}$  as active site in  $VNbO_5$  seems very small [68], although Nb in Mo-V-Nb oxide was found to inhibit the total oxidation of ethane to carbon oxides [69]. Therefore the catalytic properties of VNbPd are mainly due to vanadium oxide (eventually doped with Pd) besides  $VNbO_5$ . It may be inferred that  $(Pd)VO_x$  is responsible for high selectivity to acetic acid, possibly by making easier the selective oxidation of ethylene [6,10,21].

In our MoV-based catalysts, Mo- (according to bulk stoichiometry) and/or V-oxides (according to surface stoichiometry) are necessarily present besides the  $\theta$ -phase. According to most patents, the convenient range of Mo/V/Nb ratios is 1/0.25-0.40/0.10-0.12, and it seems nearly impossible for an unique phase to be responsible for catalytic properties. However, the two MoV-based oxides known to have a definite composition, M1 and M2, and claimed to be highly active and selective in the (amm)oxidation of propane to acrylonitrile or acrylic acid [30,31,35-37], give the opportunity to compare with our results.

#### *Comparison of MoV(NbPd) catalysts with MoV-based M1, M2 oxides*

At this point, it becomes necessary to consider the role of channel structures. In this work, two compounds with a channel structure have been evidenced, the hexagonal bronzes or mixed Mo,V oxides, and the disordered  $\theta$ -phase. It is important to remember

that the typical XRD ‘amorphous’ pattern of MoVNb and MoVNbPd is similar to that of  $\text{Mo}_{8.54}\text{V}_{2.47}\text{W}_{0.99}\text{O}_x$  in a BASF patent [7], but also to that of  $\text{Mo}_6\text{V}_{2.1}\text{Me}$  (Me = Cr, Fe, Bi, Al, Co, etc.) catalysts, which have been synthesized by Ueda et al. [34]. Recently, other mixed oxides with channel structures have been synthesized with the same hydrothermal technique [31], particularly  $\text{MoV}_{0.34}\text{O}_x$  which exhibits the same XRD pattern than phases of Mo-V-Te-Nb-O [70]. The authors pointed out that Te or Sb is unnecessary for the formation of this orthorhombic structure, whose framework is based on the  $[\text{MoO}_7,5(\text{MoO}_6)]$  pattern of the  $\theta$ -phase but differ in the way they are linked together. When Te(Sb) is added [32,33,35,36,71-73], the crystallisation of orthorhombic M1 ( $\text{Mo}_{7.5}\text{V}_{1.5}\text{NbTeO}_{29}$ ) and of hexagonal M2 ( $\text{Mo}_6\text{Te}_2\text{VO}_{20}$ ) is observed. According to Vitry et al. [70], the XRD patterns of  $\text{MoV}_{0.34}\text{O}_x$ ,  $\text{MoV}_{0.44}\text{Te}_{0.1}\text{O}_x$  and  $\text{MoV}_{0.3}\text{Nb}_{0.12}\text{Te}_{0.23}\text{O}_x$  exhibit characteristic peaks at  $2\theta = 6.6, 7.9, 9.0, 22.2, 27.3$  and  $45.3^\circ$ . Because of the amorphous state of our MoVNb(Pd) catalysts, the presence of M1 and/or M2 cannot be verified. These phases being synthesized by hydrothermal methods followed by heat treatment in lean oxygen atmosphere, we doubt that they could be formed in the ‘simple’ conditions of preparation we used, the more so because a higher content of vanadium is present in our (MoVNb) catalysts. Other authors claim that Te is necessary to get the M2 phase in cooperation with the  $\theta$ - $\text{Mo}_5\text{O}_{14}$ , association which is responsible for high yields of ethylene in ODH of ethane [72,73]. Finally, the role of Pd is worth mentioning. Adding Pd as a promoter cannot result in the same properties as adding Te (or Sb), although their basicity lies in the same range ( $\Lambda = 1.10$ - $1.18$ ) [63, 64]. Palladium (II) is a large metallic cation with a stable oxidation state in usual conditions, while  $\text{Te}^{6+}$ ,  $\text{Sb}^{5+}$  are small ( $r = 0.60$ - $0.56 \text{ \AA}$ ), non-metallic, versatile redox cations, exhibiting various valences and coordinations.

Moreover, the operating conditions (on which the actual oxidation states of the active sites at the steady state depend), the kinetic paths [11] and the chemical nature of both reactants and products, are very different. This makes it difficult to say at first that M1, M2 and the like should be better industrial catalysts for ethane oxidation to acetic acid than those we studied. Typically, the oxidation of propane is carried out close to 350-380°C, using an oxidizing gaseous mixture ( $C_3/O_2 > 1:1$ ). As the C=C bond is already present, propene is a useful (adsorbed) intermediate molecule to make acrylic acid from propane, whereas ethylene is mostly produced in a parallel way to acetic acid (at low temperature) [21,22]. The ODH of propane or ethane are currently performed at higher temperature (400-550°C) and in a reducing mixture ( $C_2/O_2 < 1:1$ ). In order to get a high enough yield of acetic acid, the oxidation of ethane must be operated at lower temperature (250-300°) than for ODH, as already demonstrated [4, 6, 9, 20]. Therefore, at first sight, there is no reason to find that the same catalyst is selective in these reactions. In order to classify the various reactions of oxidation of hydrocarbons, Bordes et al. [74] and Moriceau et al. [64,74-76] used the difference of ionisation energy,  $\Delta I$ , between the reactant (e.g., ethane) and the product (e.g., acetic acid), as a measure of the ‘thermodynamic’ selectivity. These  $\Delta I$  were plotted against the ‘optical basicity’  $\Lambda$  of the respective catalysts, which resulted in correlation lines for mild oxidation and total oxidation of hydrocarbons. Among 18 reactions of mild oxidation of  $C_1$ - $C_4$  alkanes and  $C_7$ - $C_8$  alkyl-aromatics in the  $\Delta I = 0.46$ - $0.92$  eV range, the  $\Delta I$  values for ethane oxidation to acetic or oxidative dehydrogenation to ethylene are 0.86 and 1.01 eV, respectively, and  $\Delta I = 0.35$  eV for propane oxidation to acrylic acid. As the slope of  $\Delta I = f(\Lambda)$  is positive, the correlation shows that in mild oxidation to acids, a less acidic catalyst is

required for ethane (to acetic acid) as compared to propane (to acrylic acid), and that a more basic catalyst is required for ODH of ethane than for its mild oxidation.

## 5. CONCLUSION

This work was devoted to the study of Mo-V-O catalysts differing by the nature of additive(s) for ethane oxidation to acetic acid and ethylene, with the aim of assigning a given role to the components of the system. The type, amount and characteristics of the oxides identified by several methods of analysis depend on the presence of Nb and/or Pd in Mo-containing catalysts. Precursors were also considered, with the hope that their composition and properties could highlight those of catalysts after calcination at 350 and 400°C. Nb-free catalysts are characterized by the presence of several crystalline oxides, among which hexagonal and orthorhombic ( $\alpha$ ) molybdenum trioxide, that have probably incorporated part of the vanadium. When added to MoV, palladium is responsible for decreasing the stability of these crystalline oxides. This is particularly the case of hexagonal  $\text{MoO}_3$  (or  $\text{h-Mo}_{1-x}\text{V}_x\text{O}_{3-x/2}$ ) which is transformed into  $\alpha\text{-MoO}_3$  (or  $\alpha\text{-Mo}_{1-x}\text{V}_x\text{O}_{3-x/2}$ ), which, in turn, is detrimental to catalytic performance. Nb-containing catalysts are almost amorphous materials that we assume to be made up of nanocrystalline  $\theta\text{-(VMoNb)}_5\text{O}_{14}$  and  $\text{Mo}_{1-x}\text{V}_x\text{O}_{3-x/2}$  oxides. The high degree of disorder in the stacking of these layered oxides is attributed to ions like Nb, Pd (and possibly V), ‘sandwiched’ between the layers if they are not inserted into the constitutive oxides. When added to MoVNb, Pd could be accommodated in the channels of the  $\theta$ -oxide structure, thereby reducing the instability of the material observed in the absence of Nb. In comparing the Mo-free VNbPd catalyst, which is highly selective to acetic acid and

CO<sub>x</sub>, to MoVNb and MoVNbPd catalysts, which are highly selective to mild oxidation products, a picture emerges that invokes synergistic effects [20,59-61] instead of the very specific properties of a given phase. Indeed, the fact that an “excess” of molybdenum and vanadium (as compared to the known  $\theta$ -V<sub>0.07</sub>Mo<sub>0.93</sub>O<sub>2.80</sub> or Nb<sub>0.09</sub>Mo<sub>0.91</sub>O<sub>2.80</sub>, and V<sub>0.13</sub>Mo<sub>0.87</sub>O<sub>2.925</sub>) is needed to ensure high catalytic performance in ethane oxidation, must also be taken into account. Patches of  $\theta$ -(VMoNb)<sub>5</sub>O<sub>14</sub> (possibly doped by Pd) could be ‘isolated’ in a (Mo,V)O<sub>x</sub> matrix. Alternatively,  $\theta$ -(VMoNb)<sub>5</sub>O<sub>14</sub> could serve as a basis stabilizing or isolating surface patches of (Mo,V)O<sub>x</sub>. In both hypotheses, the (main) active sites are probably the vanadium atoms, according to XPS analyses showing that the near-surface is slightly enriched with vanadium. In such cases, the interfaces must be coherent for the redox V<sup>5+</sup>/V<sup>4+</sup> to proceed at the boundaries between  $\theta$ -(VMoNb)<sub>5</sub>O<sub>14</sub> and (Mo,V)O<sub>x</sub>, or to help O<sup>2-</sup> diffusion to the surface [59-61]. This redox system would proceed faster with the help of Pd<sup>2+</sup>. The possibility of a complementary redox system between Mo<sup>6+</sup> and Mo<sup>5+</sup> at the steady state cannot be discarded. However, if it proceeds, the rate of reoxidation of Mo<sup>5+</sup> to Mo<sup>6+</sup> would be far enhanced by the neighboring vanadium, in the presence of which Mo<sup>5+</sup> specie are known to be fairly unstable.

## ACKNOWLEDGMENTS

L. Burylo and L. Gengembre are thanked for performing HT-XRD and XPS experiments, respectively. M. Roussel and M. Bouchard are indebted to SABIC R&D Management for financial support and approval to publish this work.

## REFERENCES

- [1] A. Bielański, M Najbar, *Appl. Catal. A: General*, 157 (1997) 223.
- [2] V.M. Bondareva, T.V. Andrushkevich, E.A. Paukshtis, *React. Kinet. Catal. Lett.* 32 (1986) 71.
- [3] J. Tichý, *Appl. Catal. A: General*, 157 (1997) 363.
- [4] E.M. Thorsteinson, T. P. Wilson, F.G. Young, P.H. Kasai, *J. Catal.* 52 (1978) 116.
- [5] R. Burch, R. Swarnakar, *Appl. Catal.* 70 (1991) 129.
- [6] M. Merzouki, E. Bordes, B. Taouk, L. Monceaux, P. Courtine, *Stud. Surf. Sci. Catal.* 72 (1992) 81.
- [7] K. Ruth, R. Kieffer, R. Burch, *J. Catal.* 175 (1998) 13.
- [8] K. Ruth, R. Kieffer, R. Burch, *J. Catal.* 175 (1998) 27.
- [9] K. Karim, Y.S. Bhat, S. Zaheer, A. Nafisah, US Patent 6,143,928 (2000); US Patent 6,114,278 (2000), to SABIC.
- [10] D. Linke, D. Wolf, M. Baerns, O. Timpe, R. Schlögl, S. Zeyß, U. Dingerdissen, *J. Catal.* 205 (2002) 16.
- [11] D. Linke, D. Wolf, M. Baerns, S. Zeyß, U. Dingerdissen, *J. Catal.* 205 (2002) 32.
- [12] A.T. Guttman, R.K., Grasselli, J. F. Brazdil, US 4 746 641 (1998), to SOHIO.
- [13] H. Hibst, L. Marosi, A. Tenten, US 5,807,531 (1998), to BASF.
- [14] M. Hatano, A. Kayou, EP 318,295 (1988), to Mitsubishi.
- [15] M. Lin, W.M. Linsen, EP 0962253 (1999) to Rohm&Haas.
- [16] T. Ushikubo, H. Nakamura, US 5,380,933 (1995) to Mitsubishi.
- [17] H. Werner, O. Timpe, D. Herein, Y. Uchida, N. Pfänder, U. Wild, R. Schlögl, *Catal. Lett.* 44 (1997) 153.
- [18] H. Vogel, R. Böhling, H. Hibst, *Catal. Lett.* 62 (1999) 71.
- [19] J.N. Al-Saedi, V.V. Giulianti, O. Guerrero-Pérez, M.A. Bañares, *J. Catal.* 215 (2003) 108.
- [20] M. Merzouki, B. Taouk, L. Tessier, E. Bordes, P. Courtine, in “New Frontiers in Catalysis” (L. Guzzi, et al., Eds.), *Stud. Surf. Sci. Catal.* 75 (1993) 753.
- [21] L. Tessier, E. Bordes, M. Gubelmann-Bonneau, *Catal. Today*, 24 (1995) 335.

- [22] M. Roy, M. Gubelmann-Bonneau, H. Ponceblanc, J.C. Volta, *Catal. Lett.* 42 (1996) 93.
- [23] D.I. Enache, E. Bordes-Richard, A. Ensuque, F. Bozon-Verduraz, *Appl. Catal. A : General*, 278 (2004) 93.
- [24] D.I. Enache, E. Bordes-Richard, A. Ensuque, F. Bozon-Verduraz, *Appl. Catal. A : General*, 278 (2004) 103.
- [25] G. Centi, S. Perathoner, F. Trifiró, *Appl. Catal. A : General*, 157 (1997) 143.
- [26] R. Catani, G. Centi, R.K. Grasselli, F. Trifiró, *Ind. Eng. Chem., Res.* 31 (1992) 107.
- [27] O. Mougin, PhD thesis, University of Toulouse, France (2001).
- [28] M. Bouchard, M. Roussel, E. Bordes-Richard, K. Karim, S. Al-Sayari, *Catal. Today*, 99 (2005) 77.
- [29] M. Aouine, J.L. Dubois, J.M.M. Millet, *Chem. Commun.* (2001) 1180.
- [30] J.M.M. Millet, H. Roussel, A. Pigamo, J.L. Dubois, J.C. Dumas, *Appl. Catal. A: General*, 232 (2003) 77.
- [31] T. Katou, D. Vitry, W. Ueda, *Chem. Lett.* 32 (2003) 1028.
- [32] D. Vitry, Y. Morikawa, J.L. Dubois, W. Ueda, *Appl. Catal. A: General*, 251 (2003) 411.
- [33] *Topics Catal.* 23 (2003): papers therein.
- [34] W. Ueda, K. Oshihara, *Appl. Catal. A: General*, 200 (2000) 135.
- [35] P. De Santo Jr., D.J. Buttrey, R.K. Grasselli, C.G. Lugmair, A.F. Volpe, B.H. Toby, T. Vogt, *Topics Catal.* 23 (2003) 23.
- [36] P. De Santo Jr., D.J. Buttrey, R.K. Grasselli, C.G. Lugmair, A.F. Volpe, B.H. Toby, T. Vogt, *Z. Krist.* 219 (2004) 152.
- [37] R.K. Grasselli, J.D. Burrington, D.J. Buttrey, P. De Santo Jr., C.G. Lugmair, A.F. Volpe, T. Weing, *Topics Catal.* 23 (2003) 5.
- [38] G. Mestl, Ch. Linsmeier, R. Gottschall, R. Dieterle, J. Find, D. Herein, J. Jäger, Y. Uchida, R. Schlögl, *J. Molec. Catal. A: Chemical*, 162 (2000) 463.
- [39] M. Dieterle, G. Mestl, J. Jäger, Y. Uchida, H. Hibst, R. Schlögl, *J. Molec. Catal. A: Chemical*, 174 (2001) 169.
- [40] Y. Uchida, G. Mestl, O. Ovsitser, J. Jäger, A. Blume, R. Schlögl, *J. Molec. Catal. A: Chemical*, 187 (2002) 242.

- [41] S. Knobl, G.A. Zenkovets, G.N. Kryukova, O. Ovsitser, D. Niemeyer, R. Schlögl, G. Mestl, *J. Catal.* 215 (2003) 177.
- [42] L. Dupont, D. Larcher, M. Touboul, *J. Solid State Chem.*, 143 (1999) 41.
- [43] Y. Hu, P.K. Davies, *J. Solid State Chem.*, 119 (1995) 176.
- [44] T. Eckström, M. Nygren, *Acta Chem. Scand.* 26 (1972) 1836.
- [45] G. Mestl, *J. Raman Spectrosc.* 33 (2002) 333.
- [46] R. Murugan, H. Chang, *J. Chem. Soc., Dalton Trans.* (2001) 3125.
- [47] J.M. Amarilla, B. Casal, J.C. Galvan, E. Ruiz-Hitzky, *Chem. Mater.* 4 (1992) 62.
- [48] F. Barbieri, D. Cauzzi, F. De-Smet, M. Devillers, P. Moggi, G. Predieri, P. Ruiz, *Catal. Today*, 61 (2000) 353.
- [49] N. Ballarini, G. Calestani, R. Catani, F. Cavani, U. Cornaro, C. Cortelli and M. Ferrari, *Stud. Surf. Sci. Catal.* 155 (2005) 81.
- [50] L. Dambies, C. Guimon, S. Yiacoumi, E. Guibal, *Colloid Surf. A*, 177 (2001) 203.
- [51] D. Kim, S.V. Kagwade, C.R. Clayton, *Surf. Interf. Anal.*, 26 (1998) 155.
- [52] P. Botella, J.M. Lopez-Nieto, B. Solsona, A. Mifsud, F. Marquez, *J. Catal.*, 209 (2002) 445.
- [53] <http://www.lasurface.com/>
- [54] <http://www.srdata.nist.gov>
- [55] J.P. Nogier, M. Delamar, *Catal. Today*, 20 (1994) 109.
- [56] I.E. Wachs, J.M. Jehng, W. Ueda, *J. Phys. Chem. B*, 109 (2005) 2275.
- [57] R.D. Shannon, *Acta Cryst. Sect. A*, 32 (1976) 751.
- [58] J.L. Callahan, R.K. Grasselli, *AIChE J.* 9 (1963) 755.
- [59] E. Bordes, P. Courtine, *Appl. Catal. A: General*, 157 (1997) 45.
- [60] E. Bordes, P. Courtine, *Stud. Surf. Sci. Catal.*, 110 (1997) 177.
- [61] E. Bordes, *Top. Catal.*, 15 (2001) 131.
- [62] E. Bordes, *Stud. Surf. Sci. Catal.*, 67 (1991) 21.
- [63] A. Leboutellier, P. Courtine, *J. Solid State Chem.*, 137 (1998) 94.

- [64] P. Moriceau, A. Leboutellier, E. Bordes, P. Courtine, *Phys. Chem. Chem. Phys.*, 1 (1999) 5735.
- [65] J.L. Seoane, P. Boutry, R. Montarnal, *J. Catal.*, 63 (1980) 191, 202.
- [66] E. Bordes, *Catal. Today*, 1 (1987) 499.
- [67] E. Bordes, *Catal. Today*, 3 (1987) 163.
- [68] R.H.H. Smits, K. Seshan, J.R.H. Ross, L.C.A. van den Oetelaar, J.H. Helwegen, M.R. Anatharaman, H.H. Brongersma, *J. Catal.*, 157 (1995) 584.
- [69] O. Desponds, R.L. Keiski, G.A. Somorjai, *Catal. Lett.*, 19 (1993) 17.
- [70] T. Katou, D. Vitry, W. Ueda, *Catal. Today*, 91-92 (2004) 237.
- [71] D. Vitry, J.L. Dubois, W. Ueda, *J. Molec. Catal. A: Chemical*, 220 (2004) 67.
- [72] P. Botella, E. García-González, A. Dejoz, J. M. López Nieto, M. I. Vázquez and J. González-Calbet *J. Catal* 225 (2004) 428.
- [73] J.M. López-Nieto, P. Botella, P. Concepción, A. Dejoz, M.I. Vasquez, *Catal. Today* 91-92 (2004) 241.
- [74] E. Bordes, P. Courtine, in “Metal Oxides: Chemistry Applications”, J.L.G. Fierro Ed., Marcel Dekker, p. 319.
- [75] P. Moriceau, B. Taouk, E. Bordes, P. Courtine, *Catal. Today*, 61 (2000) 197.
- [76] P. Moriceau, B. Taouk, E. Bordes, P. Courtine, P., *Stud. Surf. Sci. Catal.*, 130 (2000) 1811.

## Table captions

Table 1. Main phases and characteristics of XRD patterns and Raman spectra for catalysts calcined at 350 and 400°C.

Table 2. XPS experiments: Binding energies of Mo-containing catalysts calcined at 350°C and 400°C. Only the last digit is written in () for catalysts calcined at 400°C.

Table 3. XPS experiments: Atomic ratios and stoichiometry of Mo-containing catalysts calcined at 350°C.

Table 4. Ionic radius [57] and optical basicity  $\Lambda$  [63, 64] of some cations of interest.

Table 1.

Catalysts	XRD*	Raman
MoV-350	$\alpha$ -MoO <sub>3</sub> , Mo <sub>5</sub> O <sub>14</sub> , h-MoO <sub>3</sub> , V <sub>0.95</sub> Mo <sub>0.97</sub> O <sub>5</sub>	950-820 cm <sup>-1</sup> triplet, lines of $\alpha$ -MoO <sub>3</sub> , medium massif <i>ca.</i> 700 cm <sup>-1</sup>
MoV-400	$\alpha$ -MoO <sub>3</sub> , V <sub>0.95</sub> Mo <sub>0.97</sub> O <sub>5</sub> Mo <sub>5</sub> O <sub>14</sub>	$\alpha$ -MoO <sub>3</sub> , medium massif <i>ca.</i> 900 cm <sup>-1</sup> , medium massif <i>ca.</i> 700 cm <sup>-1</sup>
MoVPd-350	$\alpha$ -MoO <sub>3</sub> , Mo <sub>5</sub> O <sub>14</sub> , h-MoO <sub>3</sub> , V <sub>0.95</sub> Mo <sub>0.97</sub> O <sub>5</sub> , V <sub>9</sub> Mo <sub>6</sub> O <sub>40</sub>	950-820 cm <sup>-1</sup> triplet, $\alpha$ -MoO <sub>3</sub> , medium massif <i>ca.</i> 700 cm <sup>-1</sup>
MoVPd-400	$\alpha$ -MoO <sub>3</sub> , V <sub>0.95</sub> Mo <sub>0.97</sub> O <sub>5</sub>	$\alpha$ -MoO <sub>3</sub>
MoVNb-350, MoVNb-400	Nano <sup>#</sup> $\alpha$ -MoO <sub>3</sub> and nano-Mo <sub>5</sub> O <sub>14</sub>	950-820 cm <sup>-1</sup> triplet, medium massif <i>ca.</i> 700 cm <sup>-1</sup>
MoVNBpd-350 MoVNBpd-400	nano $\alpha$ -MoO <sub>3</sub> and nano-Mo <sub>5</sub> O <sub>14</sub>	950-820 cm <sup>-1</sup> triplet, medium massif <i>ca.</i> 700 cm <sup>-1</sup>
VNBpd-350, VNBpd-400	VNbO <sub>5</sub> , V <sub>2</sub> O <sub>5</sub>	V <sub>2</sub> O <sub>5</sub> and shoulders at 970 and 1017 cm <sup>-1</sup> (NbVO <sub>5</sub> )

\* Lines may be shifted as due to the incorporation of V and/or Nb, see text for more details; <sup>#</sup> Nano stands for smooth pattern (see text)

Table 2.

BE (eV)	Mo <sup>6+</sup>	V <sup>5+</sup>	V <sup>4+</sup>	Nb <sup>5+</sup>	O1s
MoV-350 (400)	232.8 (.8)*	517.6 (.9)	516.4 (.5)	-	530.7
MoVPd-350 (400)	232.8 (.4)	517.7 (.4)	516.3 (.0)	-	530.8
MoVNb-350 (400)	232.6 (.7)	517.7 (.7)	516.3 (.3)	206.9 (.9)	530.8
MoVNBpd-350 (400)	232.8 (.9)	517.7 (.9)	516.3 (.7)	207.0 (206.7)	530.8
VNBpd-350 (400)	-	517.8 (.5)	516.2 (.2)	207.2 (206.9)	530.8

Table 3.

Cat. Ref.	V/Mo	O/Mo (O/V)	Nb/Mo (V/Nb)	V <sup>5+</sup> /V <sub>tot.</sub>	Surface stoichiometry
MoV-350	0.36	3.87	-	0.83	Mo <sup>6+</sup> V <sup>5+</sup> <sub>0.30</sub> V <sup>4+</sup> <sub>0.06</sub> O <sub>3.87</sub>
MoV-400	0.50	4.18	-	0.74	Mo <sup>6+</sup> V <sup>5+</sup> <sub>0.37</sub> V <sup>4+</sup> <sub>0.13</sub> O <sub>4.18</sub>
MoVPd-350	0.40	3.86	-	0.80	Mo <sup>6+</sup> V <sup>5+</sup> <sub>0.32</sub> V <sup>4+</sup> <sub>0.08</sub> O <sub>3.86</sub> *
MoVPd-400	0.45	4.08	-	0.78	Mo <sup>6+</sup> V <sup>5+</sup> <sub>0.35</sub> V <sup>4+</sup> <sub>0.10</sub> O <sub>4.08</sub> *
MoVNb-350	0.43	4.28	0.10	0.81	Mo <sup>6+</sup> V <sup>5+</sup> <sub>0.35</sub> V <sup>4+</sup> <sub>0.08</sub> Nb <sub>0.10</sub> O <sub>4.28</sub>
MoVNb-400	0.43	4.29	0.11	0.84	Mo <sup>6+</sup> V <sup>5+</sup> <sub>0.36</sub> V <sup>4+</sup> <sub>0.07</sub> Nb <sub>0.11</sub> O <sub>4.29</sub>
MoVNbPd-350	0.59	4.57	0.08	0.76	Mo <sup>6+</sup> V <sup>5+</sup> <sub>0.38</sub> V <sup>4+</sup> <sub>0.21</sub> Nb <sub>0.08</sub> O <sub>4.57</sub> *
MoVNbPd-400	0.44	4.25	0.09	0.68	Mo <sup>6+</sup> V <sup>5+</sup> <sub>0.30</sub> V <sup>4+</sup> <sub>0.14</sub> Nb <sub>0.09</sub> O <sub>4.25</sub> *
VNbPd-350	-	(3.57)	(2.08)	0.86	V <sup>5+</sup> <sub>0.86</sub> V <sup>4+</sup> <sub>0.13</sub> Nb <sub>0.48</sub> O <sub>3.58</sub>
VNbPd-400	-	(3.70)	(2.04)	0.85	V <sup>5+</sup> <sub>0.85</sub> V <sup>4+</sup> <sub>0.15</sub> Nb <sub>0.49</sub> O <sub>3.65</sub>

\* Pd omitted; Bulk stoichiometry: MoV and MoVPd: Mo<sup>6+</sup>V<sup>5+</sup><sub>0.4</sub>O<sub>4</sub> to Mo<sup>6+</sup>V<sup>4+</sup><sub>0.4</sub>O<sub>3.8</sub>; MoVNb and MoVNbPd: Mo<sup>6+</sup>V<sup>5+</sup><sub>0.4</sub>Nb<sup>5+</sup><sub>0.12</sub>O<sub>4.30</sub> to Mo<sup>6+</sup>V<sup>4+</sup><sub>0.4</sub>Nb<sup>5+</sup><sub>0.12</sub>O<sub>4.1</sub>; VNbPd: V<sup>5+</sup>Nb<sup>5+</sup><sub>0.31</sub>O<sub>3.27</sub> to V<sup>4+</sup>Nb<sup>5+</sup><sub>0.31</sub>O<sub>2.77</sub>

Table 4.

Cation	Ionic radius (Å)	CN*	Lambda	Cation	Ionic radius (Å)	CN*	Lambda
V <sup>5+</sup>	0.355	4	0.69	V <sup>5+</sup>	0.54	6	0.63
V <sup>4+</sup>	0.58	6	0.68	V <sup>3+</sup>	0.64	6	0.55
Mo <sup>6+</sup>	0.41	4	0.55	Mo <sup>6+</sup>	0.59	6	0.52
Mo <sup>5+</sup>	0.61	6	1.17	Mo <sup>4+</sup>	0.65	6	0.96
Nb <sup>5+</sup>	0.48	4	0.64	Nb <sup>5+</sup>	0.64	6	0.61
Nb <sup>5+</sup>	0.69	7	0.60	Nb <sup>4+</sup>	0.68	6	0.81
Pd <sup>2+</sup>	0.64	4 (square)	0.85	Pd <sup>2+</sup>	0.86	6	1.11

\* CN: coordination

## FIGURE CAPTIONS

Fig. 1. XRD patterns of Nb-free precursors: P-MoV and P-MoVPd. Symbols: AHM (■);  $(\text{NH}_4)_2\text{Mo}_4\text{O}_{13}$  (◇); h-MoO<sub>3</sub> or  $(\text{NH}_4)_{0.2}\text{V}_{0.2}\text{Mo}_{0.8}\text{O}_3$  type (○)

Fig. 2. XRD patterns of Nb-containing precursors: P-VNb, P-MoVNb, and P-MoVNbPd. Symbols: V<sub>2</sub>O<sub>5</sub> (▼); NH<sub>4</sub>VO<sub>3</sub> (◇); α-MoO<sub>3</sub> (☆); θ-(MoVNb)<sub>5</sub>O<sub>14</sub> (●).

Fig. 3. Laser Raman spectrum of the three types of particles in Nb-free precursors (a-c), and of P-MoVNb and P-MoVNbPd (b). Symbols: NH<sub>4</sub>VO<sub>3</sub> (◇); V<sub>2</sub>O<sub>5</sub> (▼); α-MoO<sub>3</sub> (☆); h-MoO<sub>3</sub> or  $(\text{NH}_4)_{0.2}\text{V}_{0.2}\text{Mo}_{0.8}\text{O}_3$  type (○)

Fig. 4. Effect of laser heating on P-MoV particle. Symbols: V<sub>2</sub>O<sub>5</sub> (▼); α-MoO<sub>3</sub> (☆).

Figure 5: Effect of laser heating on P-MoVNb particle. Symbols: V<sub>2</sub>O<sub>5</sub> (▼); α-MoO<sub>3</sub> (☆).

Fig. 6. XRD patterns of MoV-based phases without and with Nb and/or Pd calcined at 350°C. Symbols: h-MoO<sub>3</sub> or  $\text{V}_{0.13}\text{Mo}_{0.87}\text{O}_{2.925}$  (○); α-MoO<sub>3</sub> (☆); θ-(MoVNb)<sub>5</sub>O<sub>14</sub> (●);  $\text{V}_{0.95}\text{Mo}_{0.97}\text{O}_5$  (□); Mo<sub>6</sub>V<sub>9</sub>O<sub>40</sub> (△).

Fig. 7. XRD patterns of MoV-based phases without and with Nb and/or Pd calcined at 400°C. Symbols: α-MoO<sub>3</sub> (☆); θ-(MoVNb)<sub>5</sub>O<sub>14</sub> (●);  $\text{V}_{0.95}\text{Mo}_{0.97}\text{O}_5$  (□).

Fig. 8. Laser Raman spectra of MoV-containing catalysts calcined at 350°C (★: MoO<sub>3</sub>)

Fig. 9. Laser Raman spectrum of MoV-containing catalysts calcined at 400°C (★: MoO<sub>3</sub>)

Fig. 10. Conversion of ethane vs. temperature of reaction for catalysts calcined at 350°C (full symbols, plain lines) and at 400°C (open symbols, dashed lines); lozenges: MoV; triangles: MoVNb; circles: MoVPd; squares: VNbPd.

Fig. 11. Selectivity to acetic acid vs. temperature of reaction for catalysts calcined at 350°C (full symbols, plain lines) and at 400°C (open symbols, dashed lines) (same symbols as Fig. 10).

Fig. 12. Selectivity to ethylene vs. temperature of reaction for catalysts calcined at 350°C (full symbols, plain lines) and at 400°C (open symbols, dashed lines) (same symbols as Fig. 10).

Fig. 13. Selectivity to mild oxidation products vs. conversion of ethane for catalysts calcined at 350°C; acetic acid: full symbols, plain lines; ethylene: open symbols, plain grey lines (same symbols as Fig. 10).

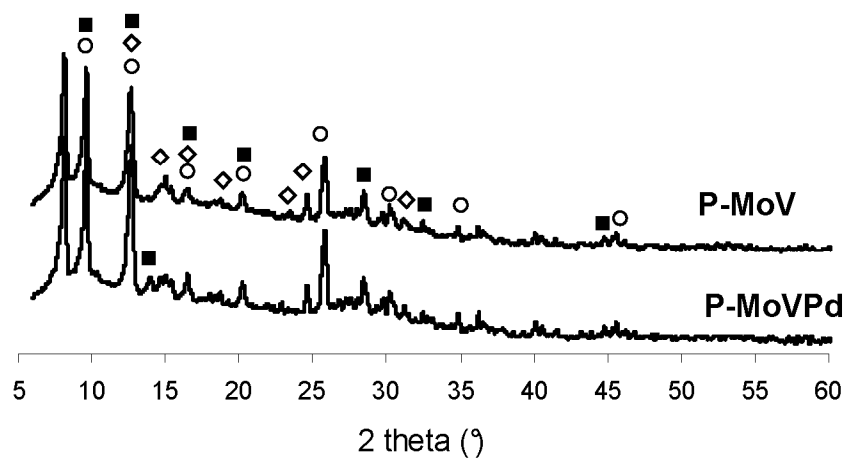


Fig. 1.

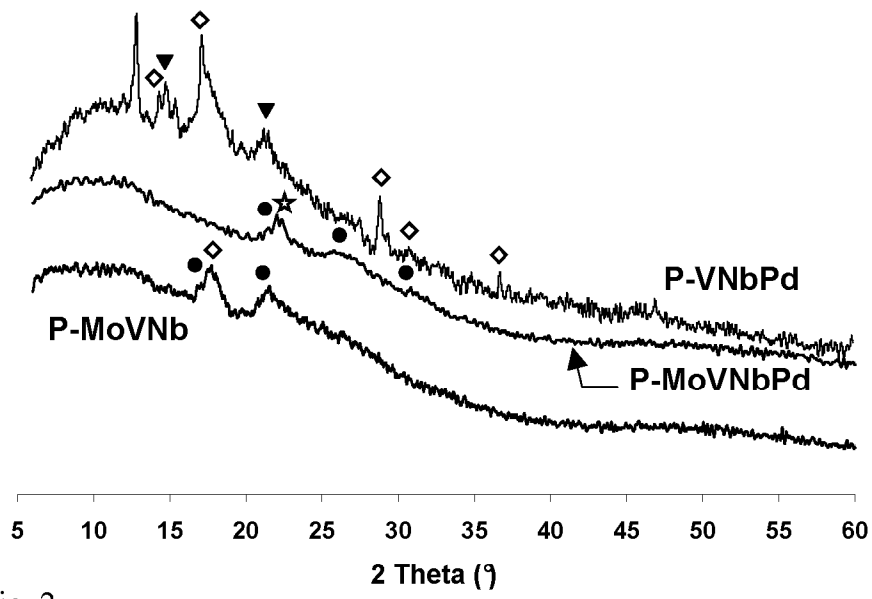


Fig. 2.

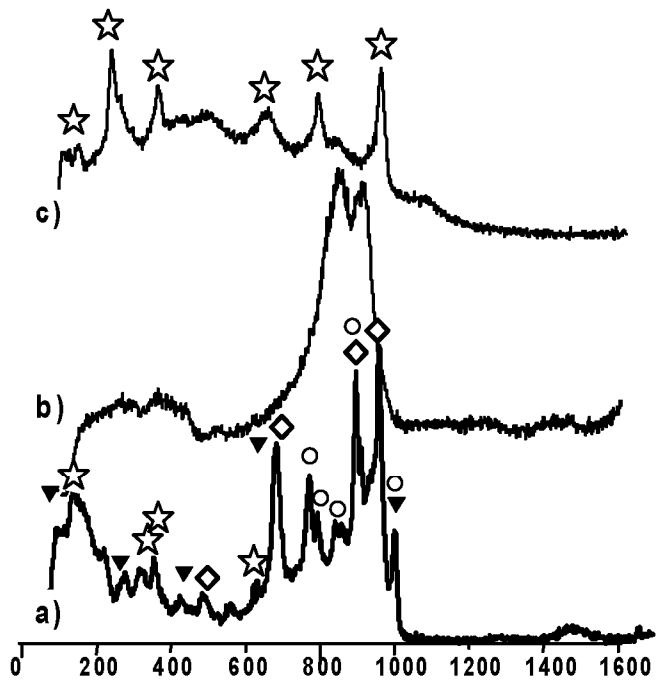


Figure 3.

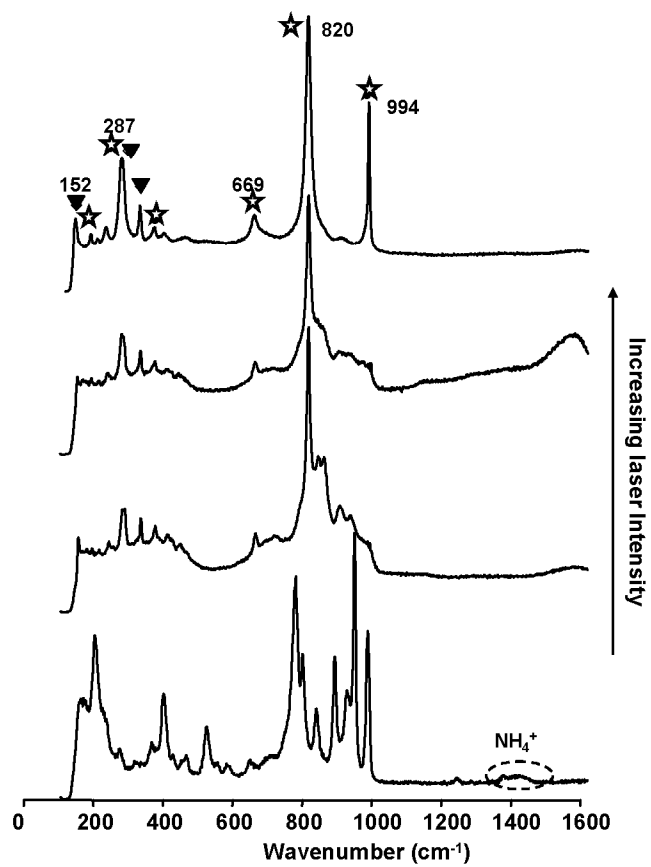


Figure 4.

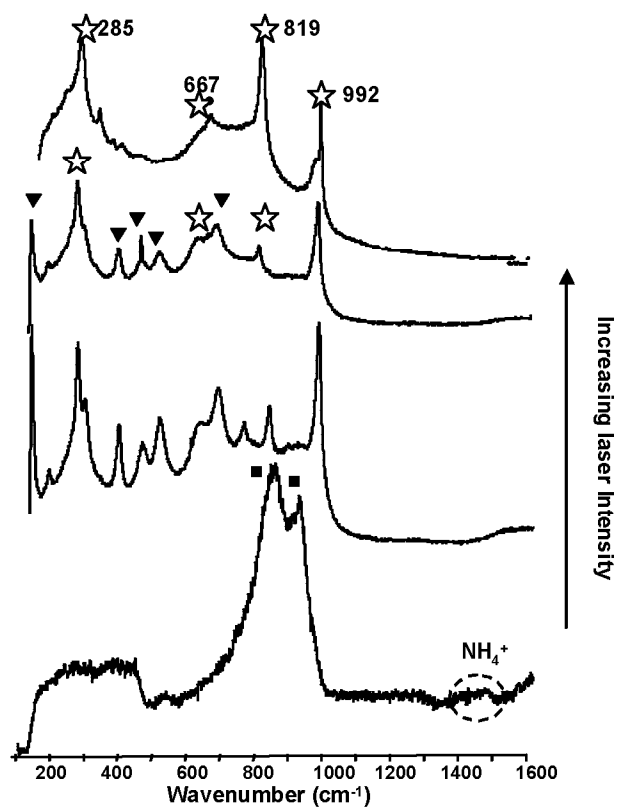


Figure 5

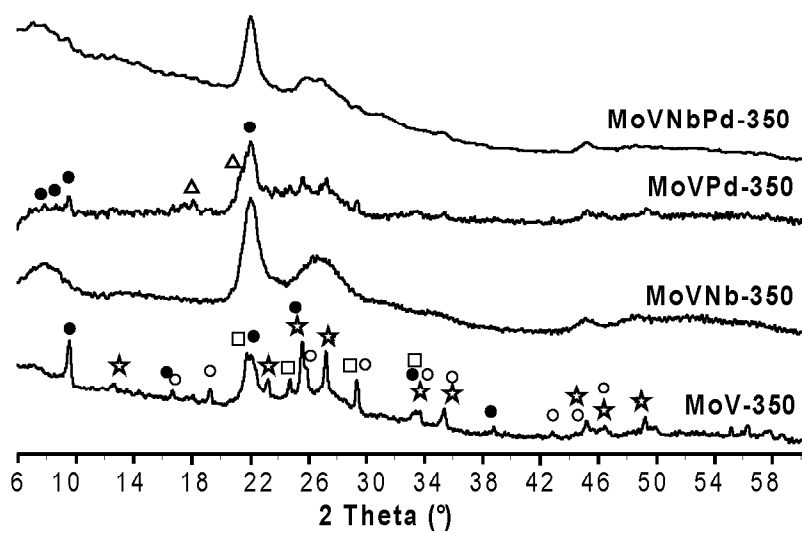


Fig. 6.

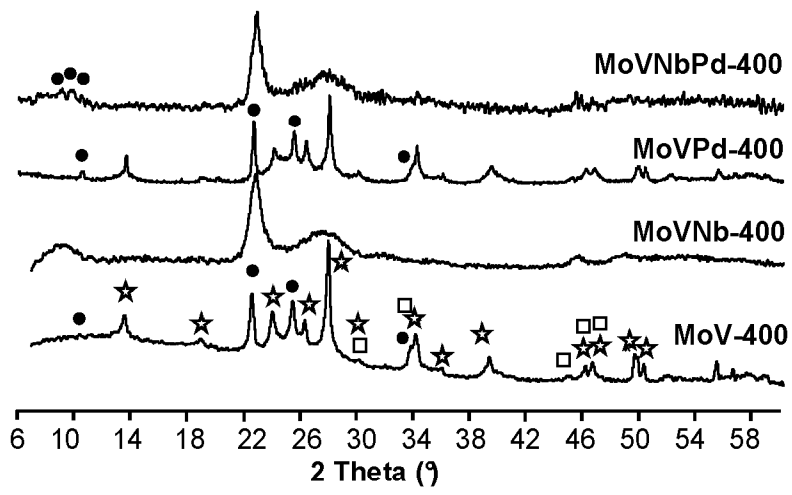


Fig. 7.

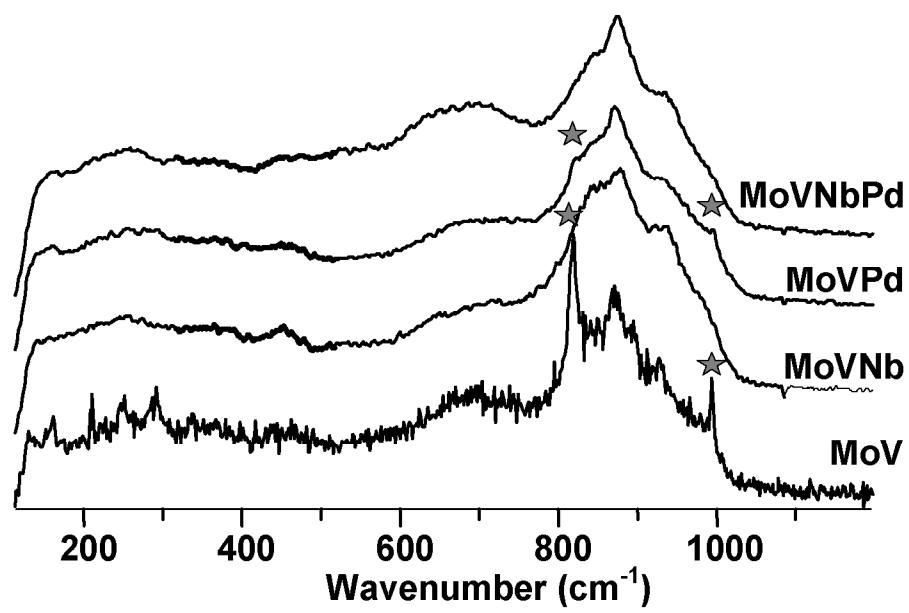


Fig. 8.

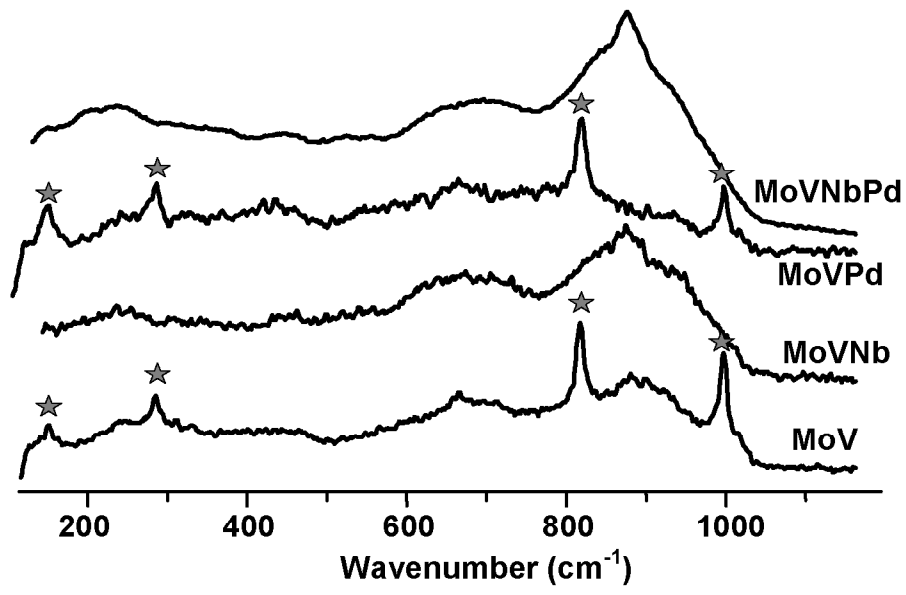


Fig. 9.

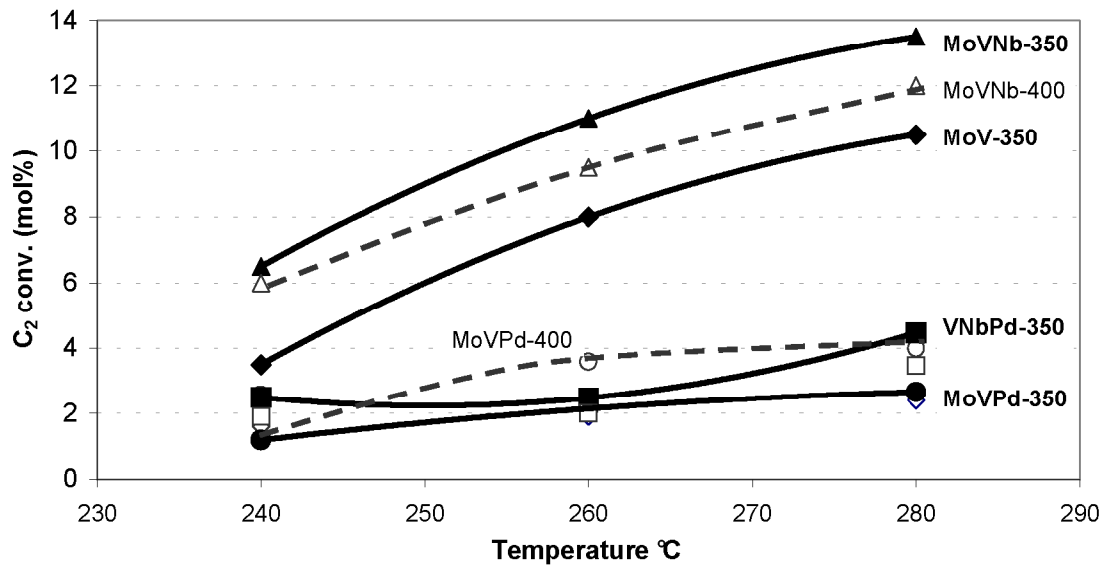


Fig. 10.

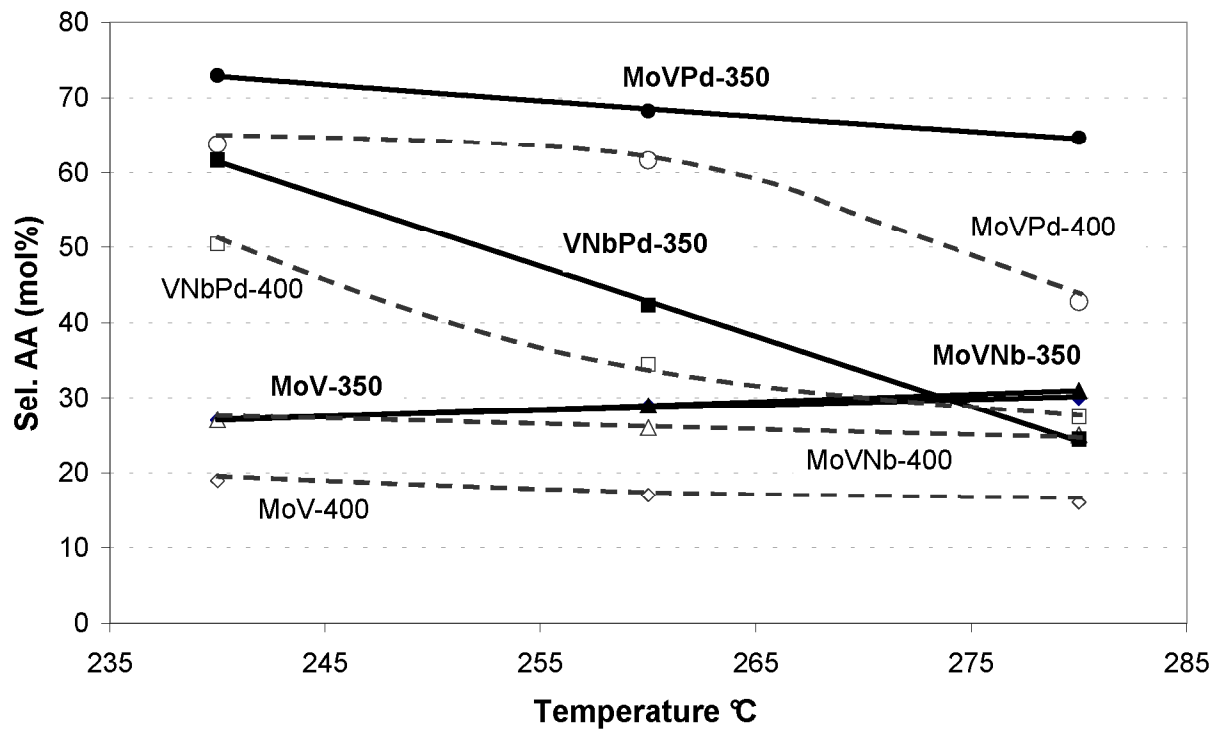


Fig. 11.

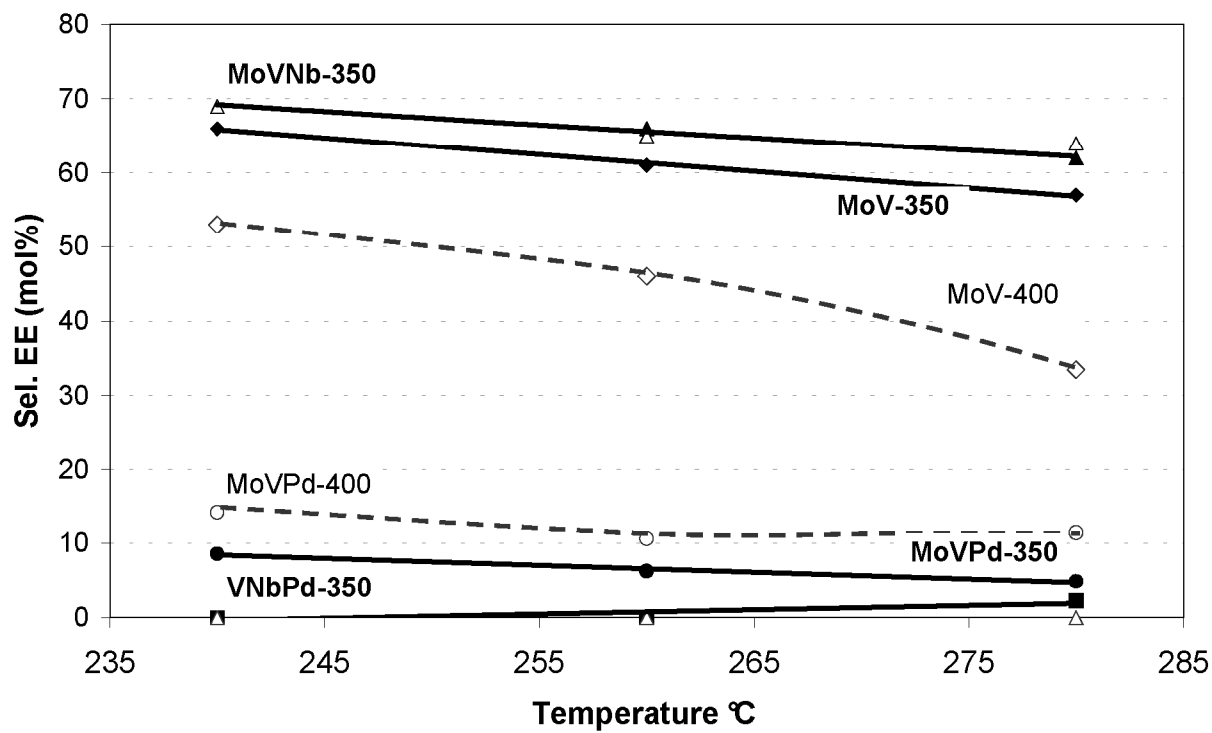


Fig. 12.

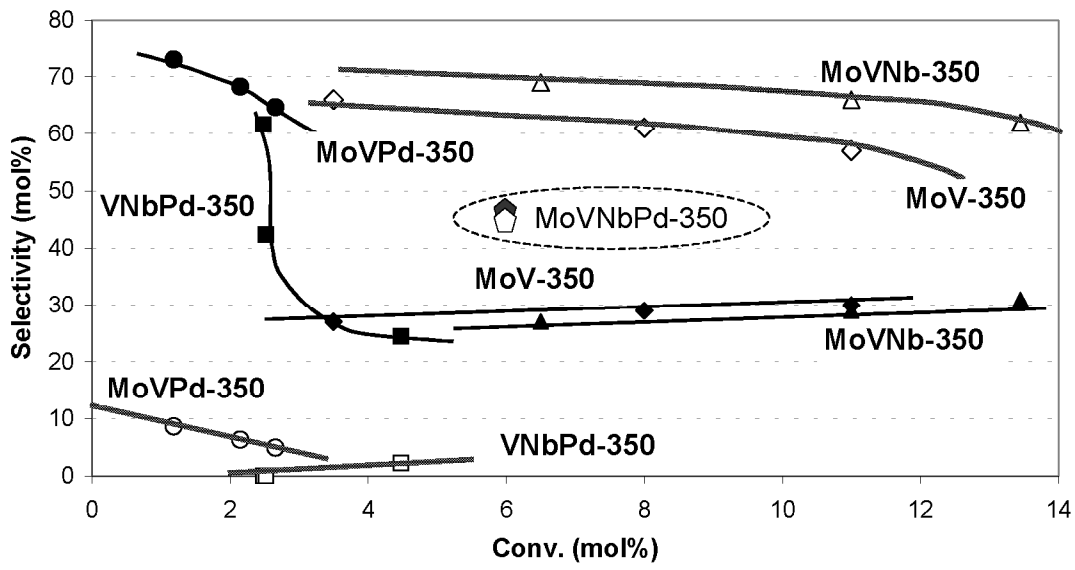


Fig. 13.